Science of the Total Environment 854 (2023) 158589

Contents lists available at ScienceDirect

Science of the Total Environment

journal homepage: www.elsevier.com/locate/scitotenv

Multiple drought indices and their teleconnections with ENSO in various spatiotemporal scales over the Mekong River Basin

Thi-Thu-Ha Nguyen [a], Ming-Hsu Li [a,*], Tue Minh Vu [b], Pei-Yuan Chen [a]

[a] Graduate Institute of Hydrological and Oceanic Sciences, National Central University, No. 300, Zhongda Rd., Zhongli District, Taoyuan City 32001, Taiwan
[b] Glenn Department of Civil Engineering, Clemson University, Clemson, SC 29631, USA

HIGHLIGHTS

- Droughts are strongly affecting the sustainability of livelihood in the Mekong River Basin.
- Multivariate drought indices are analyzed to investigate drought characteristics with different spatiotemporal scales.
- More droughts are observed in the Middle Mekong Basins.
- Higher frequency and intensity of droughts are found in the Upper Mekong Basin.
- The ENSO episodes show strong connections with droughts in the Southern Mekong River Basin.

GRAPHICAL ABSTRACT

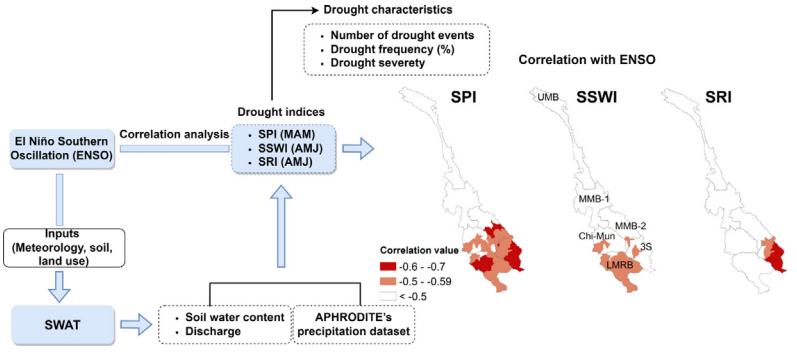

ARTICLE INFO

Editor: Fernando A.L. Pacheco

Keywords:
Mekong River Basin
Drought
El Niño Southern Oscillation index
SWAT

ABSTRACT

Drought may lead to severe and diverse impacts on agriculture, economy, and society across different regions and periods, posing predictive and adaptive challenges. In recent years, severe droughts have affected >60 million people in the Mekong River Basin (MRB). Additionally, El Niño Southern Oscillation (ENSO) episodes had distinct influences on the occurrence and intensity of drought variability in the regions. Understanding the spatiotemporal characteristics of droughts across the MRB is critical to improving management and mitigation actions. This study aims to investigate spatiotemporal drought characteristics in the MRB and their teleconnection with the ENSO. Three multiple drought indices, including the Standardized Precipitation Index (SPI) for meteorological drought, Standardized Soil Water Index (SSWI) for agricultural drought, and Standardized Runoff Index (SRI) for hydrological drought were calculated to quantify drought events, drought frequency, and drought severity. The overall patterns showed more events and larger intensity were identified by the SPI than those by the SRI or the SSWI, while the higher frequency was observed by the SRI. The Middle Mekong basins seem to experience more drought events, while higher levels of frequency and intensity of droughts were observed in the Upper Mekong Basin. The correlation analysis between ENSO index and precipitation suggested that the strongest ENSO events in Dec-Jan-Feb may result in developments of meteorological drought in Mar-Apr-May, and further led to hydrological and agricultural drought in Apr-May-Jun. Such ENSO effects had significant influences on drought variabilities in southern MRB and were insignificant in the north. The multiple drought indices show skills in identifying spatial and temporal drought characteristics from meteorological, agricultural, and hydrological perspectives, and potential for drought outlook further considering their ENSO teleconnections. The results can be applied to the development of drought monitoring methods and adaptive strategies to mitigate drought impacts through scientific and quantitative assessments.

* Corresponding author at: No. 300 Zhongda Rd., Zhongli District, Taoyuan City 320, Taiwan.
E-mail addresses: nttha@g.ncu.edu.tw (T.-T.-H. Nguyen), mli@cc.ncu.edu.tw (M.-H. Li), tuev@g.clemson.edu (T.M. Vu), pychen@ncu.edu.tw (P.-Y. Chen).

http://dx.doi.org/10.1016/j.scitotenv.2022.158589
Received 16 May 2022; Received in revised form 3 September 2022; Accepted 3 September 2022
Available online 7 September 2022

1. Introduction

Drought is considered to be one of the most complex natural hazards causing significant economic, social, and environmental losses and impacts around the world (Wilhite, 2000). The water shortage caused by persistent periods of drought lasting from several months to several years is a major challenge for the sustainability of society. As a consequence of climate change, the possibility of widespread droughts with increased frequency, severity, and duration will further magnify such impacts in developing countries (Konapala et al., 2020; Loc et al., 2021). The Mekong River Basin (MRB) is one of the most important transnational rivers in Asia, providing abundant services in biodiversity, water resources, hydropower, transportation, and agricultural production. Droughts have caused vast agricultural losses and water shortages in the lower MRB, which damaged over 104,000 ha of rice in the Vietnamese Mekong delta and affected 14 out of 24 provinces in Cambodia from 2004 to 2005 (Cosslett and Cosslett, 2018). Streamflow was found significantly decreased in recent years, resulting in the exaggeration of drought in the MRB (Keovilignavong et al., 2021; Lu and Chua, 2021), and having detrimental impacts on water resources, economy, environment, and crop production (Kang et al., 2021; Son et al.2012; Zhang et al., 2014). The extreme drought from 1990 to 1992 affected rice productivity in Thailand, causing an estimated total loss of 210 million USD in Thailand (Prapertchob et al., 2007), and 85 % of the Vietnamese Mekong Delta were affected by this event, leading to salinity intrusion and water scarcity (Lee and Dang, 2019). Another extreme drought occurred in Vietnam from 1997 to 1998, which influenced three million people and caused economic losses of up to 400 million USD in crop production (Nguyen and Shaw, 2011), affecting 30 % area of rice, and 10 % area of coffee in central highland Vietnam (Tum et al., 2016). In 2002, a severe drought event destroyed >100,000 ha of paddy fields in Cambodia, resulting in significant reductions in rice productivity in eight provinces, including Takeo, Kampong Speu, Kandal, Kampong Cham, Svay Rieng, Oddar Meanchey, Pursat, and Battambang (Nguyen and Shaw, 2011). Projections of climate simulations showed the MRB is expected to experience more severe and intensified droughts under the impacts of climate change (Dong et al., 2022; Li et al., 2021b; Mondal et al., 2021; Thilakarathne and Sridhar, 2017), and thus understanding spatiotemporal characteristics of MRB droughts is critical to decision making for planning and implementation of proper adaptation measures.

Due to the temporal development of dry spells, meteorological, agricultural, and hydrological droughts can be subsequently developed for a longer time. Meteorological drought is caused by below-normal precipitation; agricultural drought is defined as the soil water content falling below long-term mean levels; and hydrological drought occurs when river streamflow and water stored in aquifers, lakes, or reservoirs fall below long-term mean levels (Wilhite and Glantz, 1985). Table 1 lists recent studies focused on different types of historical droughts with various indices in the Mekong River Basin. The Standardized Precipitation Index (SPI) was used to assess meteorological drought in the lower MRB, showing this region experienced multiyear droughts in 1991–1994 and widespread impacts in the 2015–2016 event (Guo et al., 2017). Another study using the SPI in the Vietnamese Mekong Delta found a spatial shift of meteorological drought toward coastal provinces in the last ten years (Lee and Dang, 2019). Long-term trends and inter-annual variability of meteorological and hydrological droughts were analyzed in the MRB, and the result showed distinct regional trends different from the basin-scale trends in droughts (Liu, 2020). Meteorological, agricultural, and multivariate aspects of droughts were investigated by Kang et al. (2021) using the Modified Palmer Drought Severity Index (MPDSI), Standardized Soil Moisture Index (SSI), and Multivariate Standardized Drought Index (MSDI), respectively, showing the worst drought events were in 1991–1994 and 2015–2016, and occurring in the Upper, Mid regions of the lower MRB and 3S region. The linkages between rice productivity and meteorological and hydrologic drought variabilities over Cambodia (lower MRB) from 2000 to 2016 were examined to investigate the impacts of drought on crop yields, indicating the lower rice yields in the water-stress province (southeast regions) of Cambodia (Abhishek et al., 2021). The impacts of climate change on future meteorological droughts in the MRB were assessed by using SPI and SPEI and found the upper and middle MRB will likely experience more droughts in the near future (Dong et al., 2022; Li et al., 2021b). Most previous studies have contributed to understanding historical droughts mainly over part of the MRB with meteorological and/or agricultural droughts. Further studies for multiple droughts in the MRB are needed, such as investigating linkages among meteorological, agricultural, and hydrological droughts, with their spatiotemporal distributions.

Meteorological and hydrological data were essential to the calculation of drought indices shown in Table 1. Due to the limitation of sparse observations, hydrological models were often used to provide quantitative estimations of spatiotemporal runoff and soil water values. Based on the model's applicability, adaptability, features, capacity, and ability, multiple criteria for selecting deterministic hydrological models were developed by Cunderlik (2003) for the assessment of water resources risk and vulnerability to changing climatic conditions. The selection of semi-distributed models was generally recommended to be a good compromise between the highly simplified hydrologic processes of lumped models and the extensive data requirements of distributed models. In another study by Kumari et al. (2021), the semi-distributed Variable Infiltration Capacity model (Liang et al., 1994) was further included for evaluation and had the best score due to its flexibility in both temporal and spatial scales, medium setup time, low need in numbers of parameters, and moderate requirements of high-resolution datasets. Various hydrological models have been used to simulate hydrological processes in the MRB, including the grid-based distributed Yamanashi Hydrological Model (Kiem et al., 2005) and VMod model (Lauri et al., 2012) and semi-distributed SLURP model (Kingston

Table 1
Recent studies on different types of historical droughts with various indices for the Mekong River Basin.

Study area	Types of droughts	Drought indices	Period	Sources
Lower Mekong Basin	Meteorological and agricultural droughts	SPI, SMDI	1981–2019	Abhishek et al., 2021
Lower Mekong Basin	Meteorological drought	PDSI	1992–2006	Fok et al., 2018
Lower Mekong Basin	Meteorological drought	SPI	1981–2016	Guo et al., 2017
Lower Mekong Basin	Meteorological drought	PDSI	2000–2011	Zhang et al., 2014
Lower Mekong Basin	Multivariate droughts	MSDI	1954–2019	Kang et al., 2021
Mekong River Basin	Meteorological, agricultural drought, and multivariate droughts	MPDSI, SSI, MSDI	1953–2016	Kang and Sridhar, 2021
Mekong delta of Vietnam	Meteorological drought	SPI	1984–2015	Lee and Dang, 2019
Mekong River Basin	Meteorological and hydrological droughts	SPI, SRI	1901–2016	Liu, 2020
Mekong River Basin	Agricultural drought	PNI	1980–2008	Palanisamy et al., 2021
Lower Mekong Basin	Agricultural drought	TVDI	2001–2010	Son et al., 2012
Lower Mekong Basin	Meteorological drought	SPI	1964–2005	Thilakarathne and Sridhar, 2017

Note: Standardized Precipitation Index (SPI), Soil Moisture Deficit Index (SMDI), Palmer's Drought Severity Index (PDSI), Modified Palmer Drought Severity Index (MPDSI), Multivariate Standardized Drought Index (MSDI), Standardized Soil Moisture Index (SSI), Standardized Runoff Index (SRI), Percent Normal Index (PNI), Temperature Vegetation Dryness Index (TVDI).

et al., 2011). In this study, the semi-distributed Soil and Water Assessment Tool (SWAT) model was adopted to simulate soil water content and runoff in the MRB. Although the score of the SWAT model calculated in the study of Cunderlik (2003) was not very attractive, the low score was mainly caused by the need for a long set-up time, difficulty of use, unable for event simulation, medium in spatial scale, extensive data demand, and not flexible in temporal scale. On the other hand, the comprehensive model structure and public domain available are the advantages of using the SWAT as pointed out by Cunderlik (2003). In addition, calibration and validation are crucial to accurately simulate hydrological processes, which the SWAT-CUP (SWAT calibration and uncertainty program, Abbaspour et al., 2007) provided a graphical module to support calibration, validation, sensitivity analysis, and uncertainty analysis for SWAT simulations. Since those disadvantages are not critical to affecting our hydrological simulations, the semi-distributed SWAT model was chosen because of having been widely used to assess long-term hydrological variations and impacts of climate change and management practices in the MRB (Krysanova and White, 2015; Tan et al., 2019; Kang et al., 2021, 2022; Kang and Sridhar, 2021).

The El Niño Southern Oscillation (ENSO), a coupled ocean-atmosphere phenomenon occurring in the Tropical Pacific Ocean, has been found to have significant teleconnection to climate variations globally (Davey et al., 2014). The Palmer's Drought Severity Index (PDSI) and ENSO indices were adopted for water level reconstruction and prediction in the lower MRB by Fok et al. (2018) and they found the time-lagged information between water level and ENSO, indicating potential applications of ENSO information for water level predictions. The strongest ENSO-precipitation relationship was found in the southern MRB during the decay year of ENSO events from 1981 to 2005 (Räsänen and Kummu, 2013). Another study by Räsänen et al. (2016) found the strong seasonal effect of ENSO on March–May precipitation in the central and southern MRB over the period between 1980 and 2013. Adopting information on teleconnections between ENSO and climate variations provides possible surrogates for detecting extreme climate events (Patricola et al., 2020; Vu and Mishra, 2016). For example, predictors developed with ENSO indices for the summer monsoon rainfall in Thailand showed forecasting skills in the post-1980 highly correlated to the strength of ENSO (Singhrattna et al., 2005). Although the significance of the ENSO-precipitation relationship has been found in the MRB, there is still lacking sufficient understanding of the spatiotemporal linkage between ENSO and various types of droughts. How the teleconnection between precipitation variability and ENSO events affects developments of meteorological, agricultural, and hydrological droughts over different spatiotemporal scales in the MRB requires further investigation. Identifying spatiotemporal characteristics of droughts associated with ENSO is essential to drought monitoring and developing adaptation measures, and thus contributes to the sustainability of local livelihoods and food security in the MRB.

This study focused on two aspects of drought characteristics with subbasin information in the MRB for a long-term period of 38 years (1970–2007): (1) analyzing spatiotemporal drought characteristics for multiple droughts in the MRB; (2) identifying the connection between ENSO and multiple drought indices. First, multiple drought indices were calculated by the Standardized Precipitation Index (SPI) with precipitation data for meteorological drought, the Standardized Soil Water Index (SSWI) with soil water content data for agricultural drought, and the Standardized Runoff Index (SRI) with runoff data for hydrological droughts. Precipitation data were obtained from a gridded precipitation product. Soil water content and runoff data were simulated by the Soil and Water Assessment Tool (SWAT) model due to the limitations of sparse observations. Spatiotemporal drought characteristics were then quantified by the number of drought events, drought frequency, and drought severity retrieved from SPI, SSWI, and SRI values. Finally, the influences of ENSO on spatiotemporal variations of multiple droughts were identified by calculating correlations between the ENSO index in Dec-Jan-Feb and the SPI in Mar-Apr-May, the SSWI and the SRI in Apr-May-Jun. Advancing our quantitative understanding of spatiotemporal variations in droughts and their ENSO teleconnections would provide valuable information for water resources management and adaptation planning in the MRB, thus minimizing the impacts of droughts in the future. The rest of the paper is organized as Section 2 describes the study area and data; Section 3 is the methodology; Section 4 presents the results; discussion and conclusions are drawn in Sections 5 and 6, respectively.

2. Study area and data

The MRB has a total drainage area of 795,000 km^2 and a main river length of over 4180 km, which flows through six countries, consisting of China, Myanmar, Laos, Thailand, Cambodia, and Vietnam (Mekong River Commission, 2005). The Mekong River originates from the Tibetan Plateau, then drains through narrow mountains before entering the floodplains of Cambodia and Vietnam (Mekong downstream region). In this study, the MRB is divided into six main subbasins (Chu et al., 2003; Thilakarathne and Sridhar, 2017), namely Upper Mekong Basin (UMB), Middle Mekong Basin 1 (MMB-1), Middle Mekong Basin 2 (MMB-2), Chi-Mun, Sekong-Sesan-Srepok subbasins (3S), and Lowlands of the MRB (LMRB) for analysis as shown in Fig. 1. The region is characterized by a complex orography with the floodplains in the south and high mountains in the north, resulting in elevations ranging from a few meters above sea level in the downstream river delta to above 6000 m in the Tibetan Plateau. Since the entire MRB encompasses high-altitude continental and temperate in the upper basin to tropical monsoonal in the lower basin (the Mekong River Commission), the annual precipitation shows remarkable spatiotemporal variability ranging from 400 mm in the northern basin to 2000 mm in the southern (Lauri et al., 2014).

The land use data of the MRB used in this study is a subset of the Global Land Cover Characteristics (GLCC) developed in 2000, by the European Commission and illustrated in Fig. 2(a). Mixed coniferous forest and cropland account for 44 % and 36 % of the MRB which is mainly observed in its downstream, and grassland covers 14 % mainly appeared in its upstream. The soil map was obtained from the Food and Agriculture Organization (FAO) in 2003 and depicted in Fig. 2(b) showing heterogeneous soil patterns observed in the MRB. In the northern part of the basin, the soil is characterized by a shallow layer consisting of clay (heavy) (20 %), sandy loam (30 %), and loamy sand (20 %). In the central and southern basins, soil types are dominated by the presence of clay loam (40 %), sandy clay loam (10 %), and clay (15 %).

Daily precipitation data from 1970 to 2007, with a spatial resolution of 0.25° × 0.25°, was extracted from the gridded precipitation product of the Asian Precipitation - Highly-Resolved Observational Data Integration Toward Evaluation (APHRODITE) dataset (Yatagai et al., 2012). APHRODITE is an observation-based precipitation dataset developed from a high-density network of rain gauges over Asia. This dataset has provided high-quality precipitation data, and was evaluated as one of the best gridded precipitation datasets for hydrological modeling purposes in the MRB (Vu et al., 2012; Lauri et al., 2014). Daily minimum and maximum temperature data, with a spatial resolution of 0.5° × 0.5°, was obtained from the Climate Prediction Center (CPC) from 1979 to 2007. Both gridded meteorological products have been applied to the MRB studies (Dang et al., 2020; Hoang et al., 2016; Lauri et al., 2014; Vu et al., 2012; Vu and Mishra, 2016). Daily river discharge data at nine river flow stations, namely Chiang Saen, Luang Prabang, Vientiane, Nakhon Phanom, Mukdahan, Pakse, Stung Treng, Kratie, and Phnom Penh were collected for the period 1966–2007 from the Mekong River Commission (MRC) as shown in Fig. 1. Oceanic Niño Index (ONI) obtained from the National Oceanic and Atmospheric Administration (NOAA), was used to represent the evolution of ENSO that will be used to investigate its teleconnections with multiple droughts in the MRB. The Niño 3.4 region is widely used for defining the phase of the ENSO by calculating sea surface temperature anomalies covering a region defined by 5°S-5°N and 170°W-120°W. The monthly ONI of the 3.4 region from 1950-present is available from the website of NOAA.

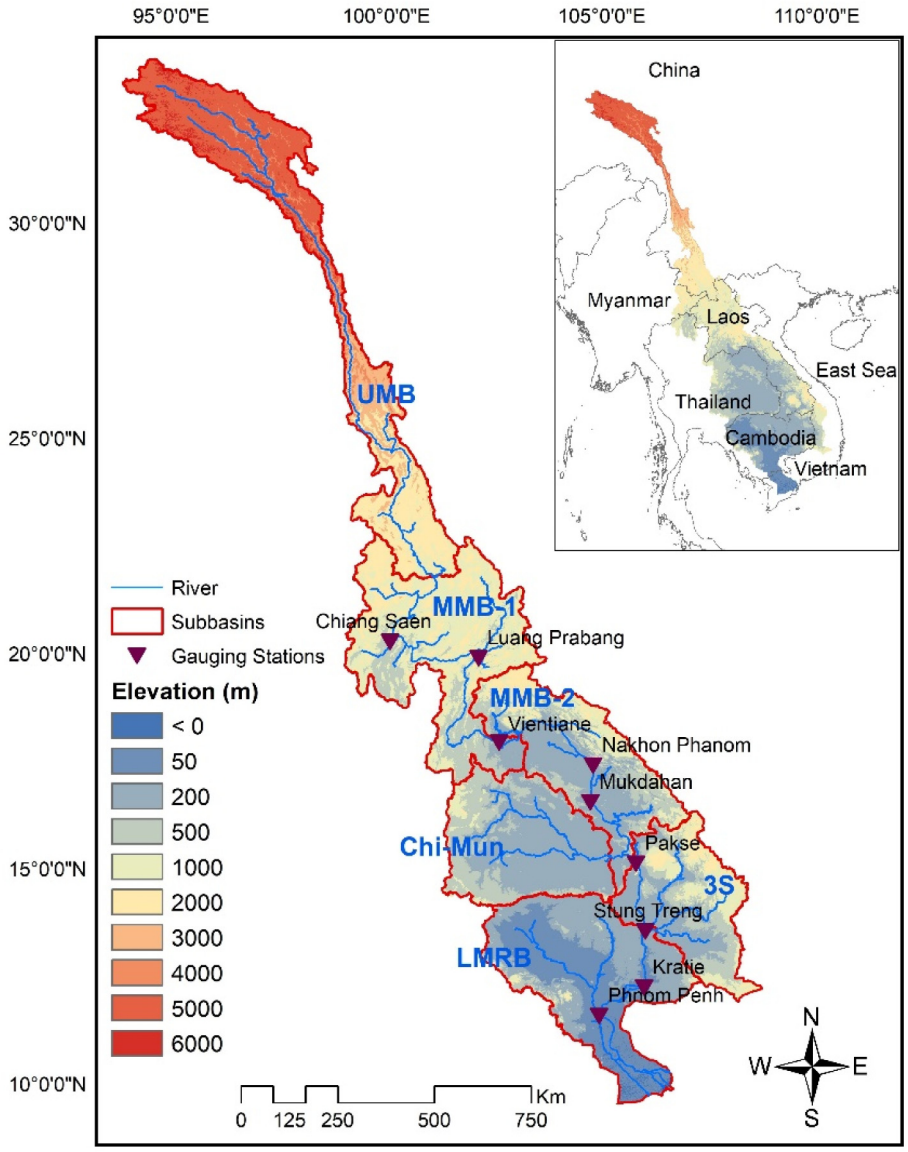

Fig. 1. Location of the Mekong River Basin, elevation, subbasins, and discharge gauging stations.

3. Methodology

3.1. Framework of the study

The framework of this study is illustrated in Fig. 3, including the SWAT simulations, the calculations of drought characteristics, and the analysis of droughts-ENSO teleconnection. Daily precipitation and temperature were used to drive the SWAT model (Arnold et al., 1998) for hydrological simulations to obtain spatiotemporal variations of hydrological data in subbasin scales. Section 3.2 provides a brief introduction to the SWAT model. The meteorological, agricultural, and hydrological droughts were identified by the Standardized Precipitation Index (SPI), the Standardized Soil Water Index (SSWI), and the Standardized Runoff Index (SRI), respectively. The SPI was computed spatially for the MRB using the APHRODITE's precipitation dataset. Due to the limitation of sparse observations in the MRB, discharge and soil water content required for calculating the SRI and SSWI were obtained by the SWAT simulations and the water balance equation. All three indices were calculated for a moving window of 6 months in 87 subbasins to analyze spatial drought characteristics, including the number of drought events, drought frequency, and drought severity. Details of these indices and the selection of the 6-month moving average are explained in Section 3.3. The teleconnection between meteorological drought and ENSO was analyzed by calculating correlations between SPI in Mar-Apr-May and ENSO index in Dec-Jan-Feb. For the ENSO teleconnections with agricultural and hydrological droughts, both SSWI and SRI in Apr-May-Jun were considered. The period of drought indices selected and their lagged relationships with ENSO were further explained in Section 3.4.

3.2. Soil and Water Assessment Tool (SWAT) hydrological model

The SWAT is a semi-distributed hydrological model developed by the United States Department of Agriculture (Arnold et al., 1998, 2012). In this study, the SWAT (version 2012) with an ArcGIS interface was adopted, and the MRB was delineated into 87 subbasins with 983 hydrological response units (HRUs). Calibrations were performed by the SWAT-CUP with a sequential uncertainty fitting (SUFI-2) (Abbaspour et al., 2007). The SUFI-2 was known as an efficient optimization algorithm with fewer model runs to achieve good simulation results (Abbaspour et al., 2004; Wu and Chen, 2015; Yang et al., 2008). Performances of the SWAT simulations were evaluated by three commonly used statistics, including Coefficient of determination (R^2), Nash-Sutcliffe index (NSE) (Nash and Sutcliffe, 1970), and Percent bias (PBIAS). According to Moriasi et al.

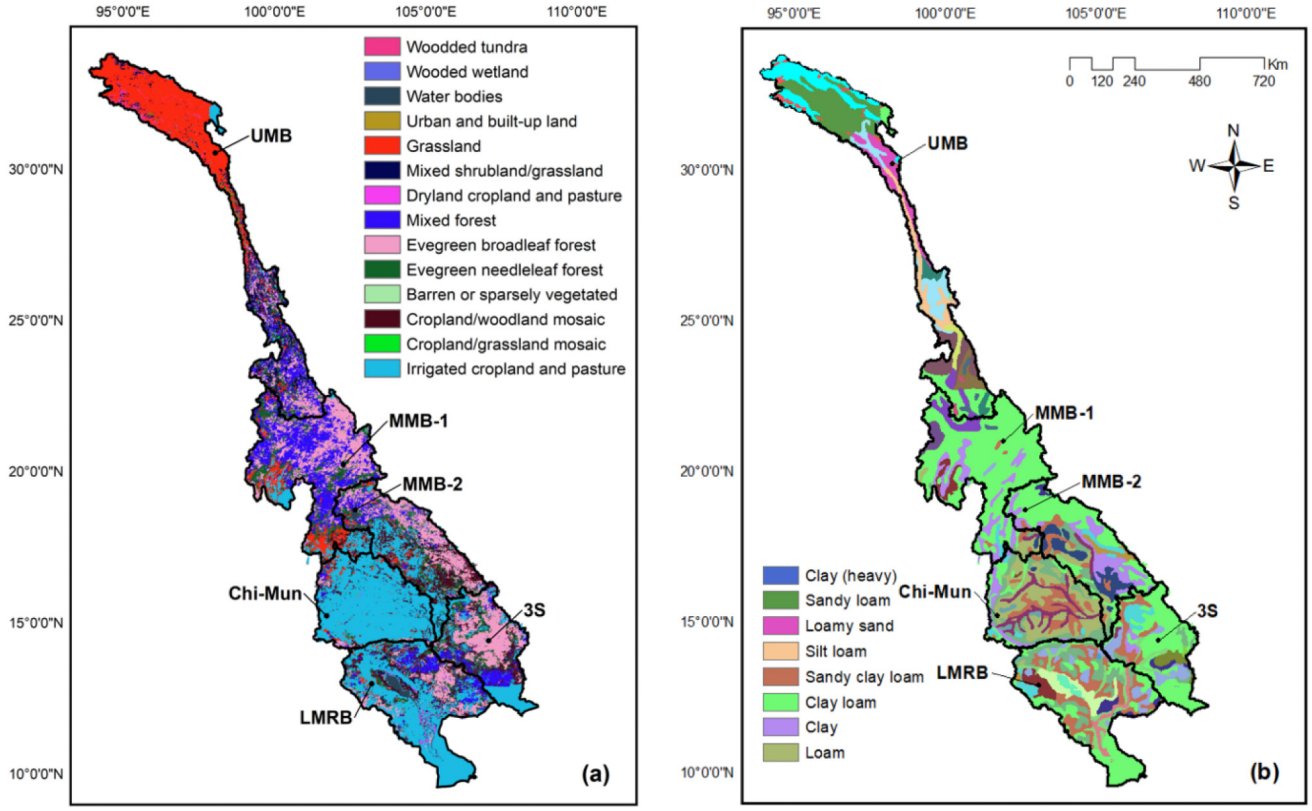

Fig. 2. (a) Land use map derived from the Global Land Cover Characterization dataset; (b) soil map retrieved from the Harmonized World Soil Database.

(2007), NSE and PBIAS are considered acceptable when values are >0.5 and less than ±25 %, respectively, for monthly streamflow.

The SWAT model was calibrated and validated for 1970–1990 and 1991–2007, respectively. Eight parameters were identified by the SWAT-CUP with the SUFI-2 method as the most sensitive parameters for auto-calibration. Sensitivity analysis is a key step in understanding how parameters affect the SWAT model performances, and to decrease the number of parameters when a calibration process is required (Li et al., 2021a). The selected sensitive parameters were determined for the calibration and validation processes based on their *p*-value (Abbaspour et al., 2007) as

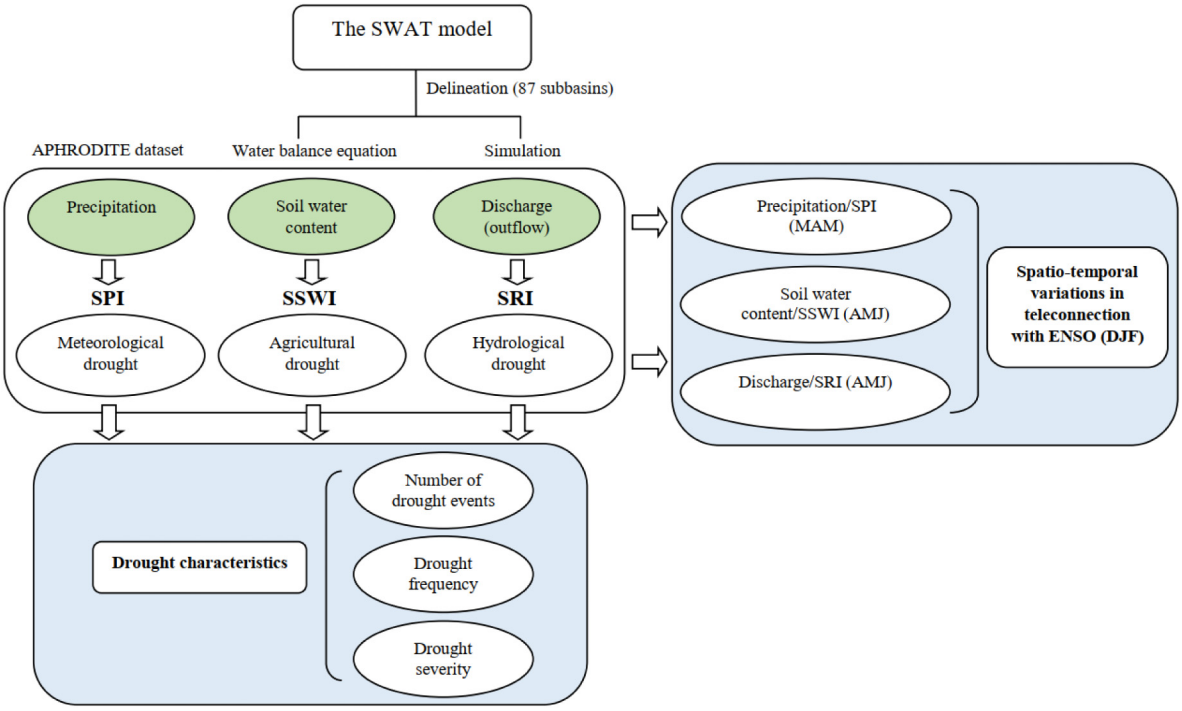

Fig. 3. The framework adopted in this study, including the data required to calculate the SPI, SSWI, and SRI, the three drought characteristics identified with these indices, and their teleconnection with the ENSO.

shown in Table A1. In this study, the most sensitive parameters were illustrated in Table 2, in which the Curve Number for moisture condition II (CN2) and groundwater delay (GW_REVAP) were calibrated with different values for each subbasin.

3.3. Drought indices

In this study, three drought indices (i.e., SPI, SRI, and SSWI) were calculated to quantify the spatiotemporal characteristics of three types of droughts (i.e., meteorological, agricultural, and hydrological droughts) in the MRB. Although there are different drought indices have been applied to drought studies in the MRB, the SPI was commonly used to investigate meteorological droughts in many studies (Table 1). By following the same statistical approach for the SPI, both the SRI and the SSWI were calculated with the outputs of the SWAT simulations to incorporate hydrological processes. As a result, both the SRI and the SSWI provide a useful complement to the SPI by using a consistent approach to identifying hydrological and agricultural aspects of droughts (Shukla and Wood, 2008; Leng et al., 2015; Vu et al., 2015a; Vu et al., 2017). Meteorological drought can be identified by the SPI with values ranging from 0 to −1, −1 to −1.5, −1.5 to −2, and less than −2 for mild, moderate, severe, and extreme drought, respectively (McKee et al., 1993). It has the advantage of detecting abnormal dryness with monthly resolutions constructed from moving windows of selected numbers of months (Guttman, 1999). Since all three indices were considered in this study, the selection of accumulation months may affect drought characteristics identified in meteorological, agricultural, and hydrological aspects. Longer accumulation periods (e.g., 12 months) will dissimulate differences among indices, while the shorter (e.g., 3 months) will induce large discrepancies such as the drought only occurred as a meteorological event (Vu et al., 2018). An accumulation period of 6 months was selected for all three indices to assess the extent of dryness from meteorological through agricultural to hydrological droughts. Precipitation data resampled from the APHRODITE's gridded data were used to calculate 6-month SPIs after fitting the Gamma distribution (Vu et al., 2017). The SSWI and SRI were evaluated with soil moisture and runoff of the SWAT simulations (Leng et al., 2015; Shukla and Wood, 2008; Vu et al., 2015a), and following the same concept used to calculate SPI. Taking the calculation of the SPI as an example, the long-term precipitation data is fitted to a Gamma distribution to determine a probability density function as shown in Eq. (1).

$$g(x) = \frac{1}{\beta^{\alpha}\Gamma(\alpha)} x^{\alpha-1} e^{-x/\beta}, \text{for x} > 0 \quad (1)$$

where $\alpha > 0$ is the shape parameter, $\beta > 0$ is the scale parameter, $x > 0$ is the amount of accumulated precipitation. $\Gamma(\alpha)$ is known as the Gamma function which is defined as the integral from Eq. (2)

$$\Gamma(\alpha) = \int_0^{\infty} y^{\alpha-1} e^{-y} dy \quad (2)$$

Table 2
Parameters and calibrated values used for the SWAT simulations in the MRB. Calibrated values with a superscript "a" represent values varying for different subbasins.

Parameter	Description and units	Range	Calibrated values
CN2	Initial SCS runoff curve number for moisture condition II	35–98	77.42–94.8[a]
GW_REVAP	Groundwater delay (days)	0.02–0.2	0.16–0.2[a]
ALPHA_BF	Baseflow alpha factor (days)	0–1	0.53
CH_K2	Effective hydraulic conductivity in main channel alluvium	−0.01-500	292
SOL_K	Saturated hydraulic conductivity	0–200	14.85
CH_N2	Manning "n" value for the main channel	−0.01-0.3	0.02
GW_DELAY	Delay time for aquifer recharge (days)	0–500	67.5
ESCO	Soil evaporation compensation factor	0–1	0.82

Once the probability density function is determined, the cumulative probability $G(x)$ can be computed by Eq. (3) to present a certain amount of precipitation that is observed for a given month at specific time scale.

$$G(x) = \int_0^{\infty} g(x) dx \quad (3)$$

The Gamma function is not defined when $x = 0$ for zero precipitation. Then, the cumulative probability of precipitation $H(x)$ is computed by Eq. (4), and q is the probability of zero precipitation.

$$H(x) = q + (1 - q)G(x) \quad (4)$$

The SPI values were obtained by transforming the cumulative probability of precipitation $H(x)$into a normal standardized distribution, with mean $\mu = 0$ and standard deviation $\sigma = 1$. The SPI is the inverse of the normal cumulative distribution function of the corresponding probability $H(x)$.

Drought characteristics were accessed in terms of drought events, drought frequency, and drought severity. Taking the meteorological drought as an example, a drought event is identified when the SPI value falls less than −1 and ends when it turns larger than −1. Drought frequency quantified the averaged probability of having droughts in a time period and was computed as the ratio of months having the SPI value less than −1 to the total number of months in the study period. Drought severity presented the total magnitude of drought over the study period and was calculated as the summation of all SPI values less than −1 for all drought events. Characteristics of agricultural and hydrological droughts were then assessed by the SSWI and SRI, respectively, following the same approach used to quantify meteorological drought. The spatial characteristics of droughts will be illustrated with results in 87 subbasins and aggregated for comparisons in 6 main subbasins as presented in the Results section.

3.4. ENSO-drought indices relationship

The spatial correlation between ENSO and drought indices of 87 subbasins is calculated by the Pearson correlation coefficient (r) and displayed with the GIS technique. The r-value close to +1 or −1 indicates a better linear relationship and shows no linear relationship when the values are closed to 0. Effects of ENSO correlation of droughts are evaluated by selecting Dec-Jan-Feb ONI as references for comparisons because the northern-hemisphere winter is usually the mature phase of ENSO events (Rasmusson and Carpenter, 1982). Past studies found the strongest influence of ENSO on dry season precipitation in East Asia, and show a high correlation of 3-month lag in lower MRB (Räsänen and Kummu, 2013; Räsänen et al., 2016). Therefore, the changes in the ENSO pattern and its teleconnections with meteorological droughts are evaluated with a 3-month lag by calculating the r values between the ONI in Dec-Jan-Feb (DJF) and the SPI in Mar-Apr-May (MAM). The variations in soil moistures and discharges in association with changes in precipitations depend on several factors, including precipitation intensity, drainage area, terrain slopes, land use, soil types, and antecedent moisture conditions. To simplify the selection of lag months in both SSWI and SRI for ENSO teleconnection analysis, the one-month lag of SSWI and SRI with respect to the SPI was selected based on a previous study analyzing long-term data showing there is a one-month lag between precipitation and discharge in the MRB (Xue et al., 2011). Thus, both agricultural and hydrological droughts were quantified with a one-month lag to the onset of meteorological droughts in this study, i.e., Apr-May-Jun (AMJ) for both SSWI and SRI values are selected to assess the effects of Dec-Jan-Feb ENSO teleconnections.

Table 3
SWAT model performance for monthly discharges during calibration and validation periods.

Station	Calibration (1970–1990)			Validation (1991–2007)		
	R^2	NSE	PBIAS (%)	R^2	NSE	PBIAS (%)
Chieang Saen	0.92	0.8	−20.1	0.94	0.9	−8.5
Luang Prabang	0.93	0.86	−18.7	0.93	0.91	−10.5
Vientiane	0.92	0.85	−20.5	0.94	0.93	−6.7
Nakhonphanom	0.93	0.92	−10.5	0.94	0.88	15.7
Mukdahan	0.92	0.92	−9.2	0.94	0.91	9.9
Pakse	0.92	0.91	−8.6	0.94	0.93	3.9
Stung Treng	0.91	0.85	11.3	0.94	0.8	24.7
Kratie	0.92	0.91	−8.6	0.94	0.92	6.1
Phnompenh	0.92	0.91	−7.1	0.95	0.95	1

4. Results

4.1. Hydrological model results

Observed station discharges were used to compare with results of hydrological simulations for model calibration and validation. Table 3 listed statistics of simulated monthly discharges during both periods. Results of SWAT hydrological simulations were acceptable with R^2 higher than 0.9, NSE ranges between 0.8 and 0.95, and PBIAS lower than ±25 %. Differences in statistics among stations were not significant. Comparisons between observed and simulated monthly discharges at Luang Prabang, Mukdahan, and Kratie stations are depicted in Fig. 4 to demonstrate monthly discharge variations from upstream to downstream MRB. The peak monthly discharges at the Mukdahan station in the MMB-2 were roughly one order larger than those at the Luang Prabang station in the MMB-1, and the peak monthly discharges at the Kratie station in the LMRB were 1.5 orders more than those at the Mukdahan station. Interannual and seasonal flow variations were well captured by the SWAT simulations, while some peak and low discharges were underestimated and overestimated, respectively.

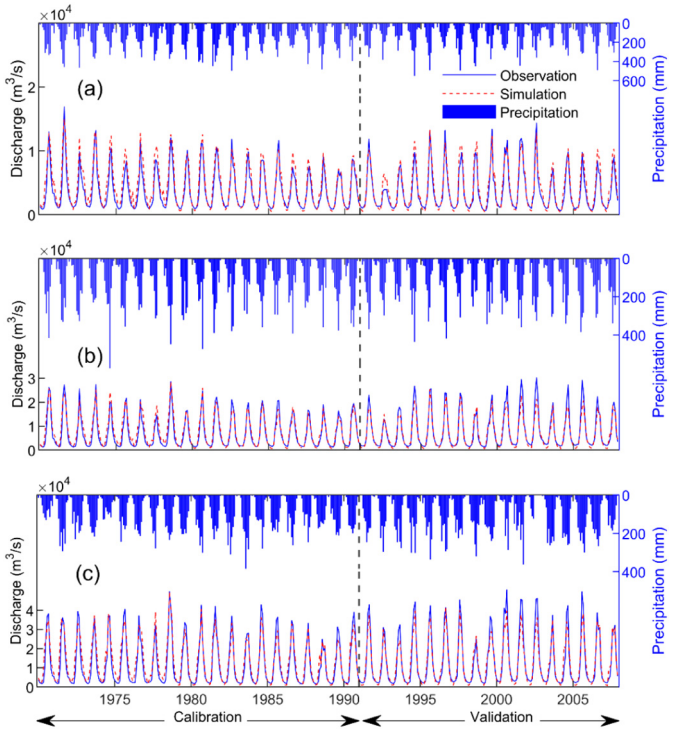

Fig. 4. Monthly observed and simulated discharge at three gauging stations. (a) Luang Prabang in the MMB-1; (b) Mukdahan in the MMB-2; (c) Kratie in the LMRB for the calibration period (1970–1990) and validation period (1991–2007).

Table 4
Annual water balance components of the MRB calculated by the SWAT during calibration and validation periods. The percentage of each component with respect to precipitation was shown in the bracket.

Water balance components (mm/year)	Calibration (1970–1990)	Validation (1991–2007)
Precipitation (PREC)	1236	1262
Groundwater flow (GWQ)	420 (34 %)	396 (31 %)
Lateral flow (LATQ)	53 (4 %)	53 (4 %)
Surface runoff (SURQ)	272 (22 %)	255 (20 %)
Evapotranspiration (ET)	459 (37 %)	524 (41 %)

The major water balance components involved in the SWAT simulations included precipitation (PREC), Groundwater flow (GWQ), Lateral flow (LATQ), Surface runoff (SURQ), and Evapotranspiration (ET). The mean annual basin values of these components and their percentages with respect to annual precipitation in the MRB during calibration and validation periods were shown in Table 4. The water loss due to the ET accounted for 37 % and 41 % of the PREC during calibration and validation periods, respectively. The contributions of GWQ from the shallow aquifer into stream discharges were larger than those of the SURQ from direct runoff during rainfall events. The LATQ from root zoon soil water played marginal contributions to streamflow. Fig. 5 showed the annual water balance components of the MRB from 1970 to 2007. The differences between the precipitation shown with the start sign and the summation of the GWQ, the LATQ, the SURQ, and the ET shown with color bars were attributed to the changes in soil water contents due to the infiltration. Spatial variability of soil water contents during drying and wetting processes was discussed in Section 5.1.

4.2. Assessing a historical extreme drought in the MRB

The 1992 extreme drought event during one of the strongest El Niño phases was considered to demonstrate the feasibilities of these drought indices to capture drought spatial variations. Drought severities were classified into five levels, including no drought, mild drought, moderate drought, severe drought, and extreme drought, as explained in Section 3.3. Drought indices were calculated for the driest month of May in 1992 as shown in Fig. 6. Northern and eastern Thailand, most of Cambodia, and southwest Vietnam had severe to extreme droughts as identified by the SPI. Moderate and severe droughts were mainly observed by SSWI and SRI in southeast Thailand, Cambodia, and southwest Vietnam. Results of the 1992 drought events observed by our multiple indices assessments were comparable to the studies by Prapertchob et al. (2007) and Nguyen and Shaw (2011), showing substantial agricultural and economic losses of 210 and 400 million USD in Thailand and Vietnam, respectively.

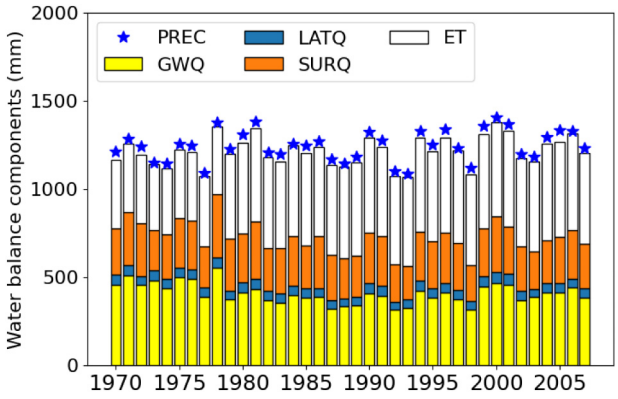

Fig. 5. Annual water balance components of the MRB from 1970 to 2007.

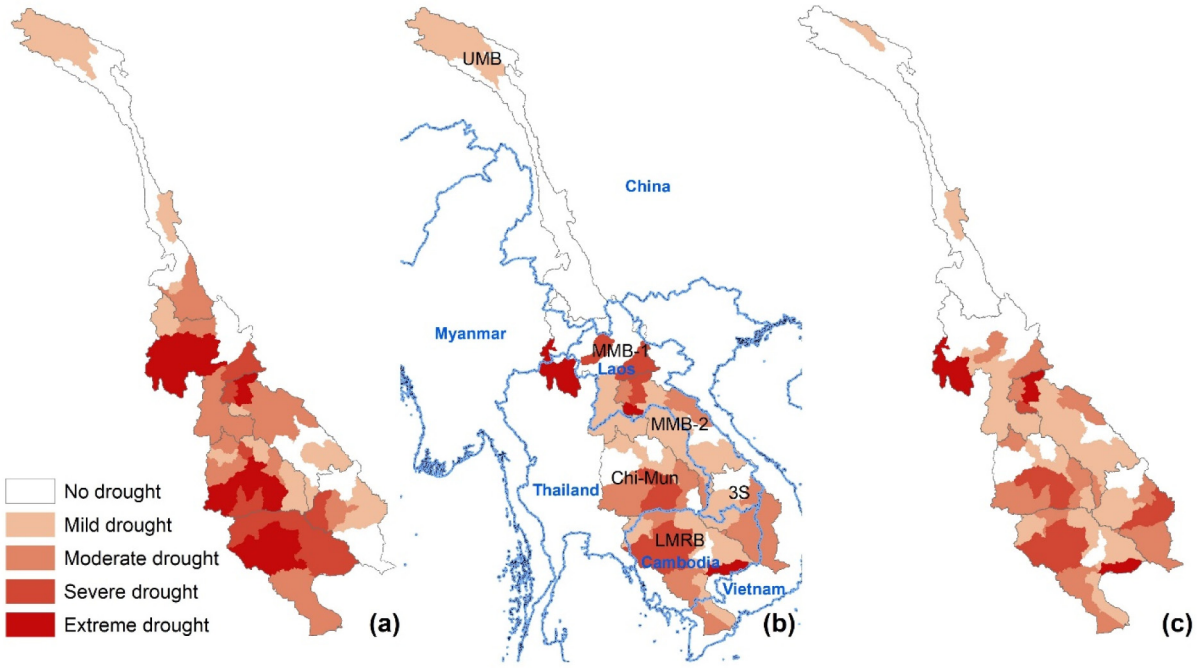

Fig. 6. Spatial distribution of drought indices in May 1992 over Mekong River Basin. (a) SPI, (b) SSWI, and (c) SRI.

4.3. Drought characteristics

4.3.1. Drought events

Spatial distributions of numbers of meteorological, agricultural, and hydrological drought events identified by SPI, SSWI, and SRI, respectively, for 87 subbasins are shown in Fig. 7. Distinct spatial variations in the number of drought events were observed, and the middle Mekong basins had a higher number of drought occurrences. The numbers of SPI events were much larger than those of SSWI and SRI events, and the numbers of SRI events were slightly greater than those of SSWI. Table 5 lists the numbers of drought events averaged in six main subbasins which showed the numbers of drought events having a general pattern of numbers of SPI events more than those of SRI and SSWI events. Since small meteorological drought events were not dry enough to induce hydrological or agricultural droughts, the SPI values were larger than the SRI and the SSWI values. Although differences between SRI and SSWI were not significant in the UMB, MMB-1, MMB-2, and 3S, the number of SRI events was greater than those of SSWI events in Chi-Mun and LMRB. As shown in Fig. 2(a), irrigated cropland and pasture cover most of Chi-Mun and LMRB, which have dense populations, causing high demand for surface water and leading to low streamflow, especially during droughts. As a result, the events of hydrological droughts were higher than those of agricultural droughts in Chi-Mun and LMRB.

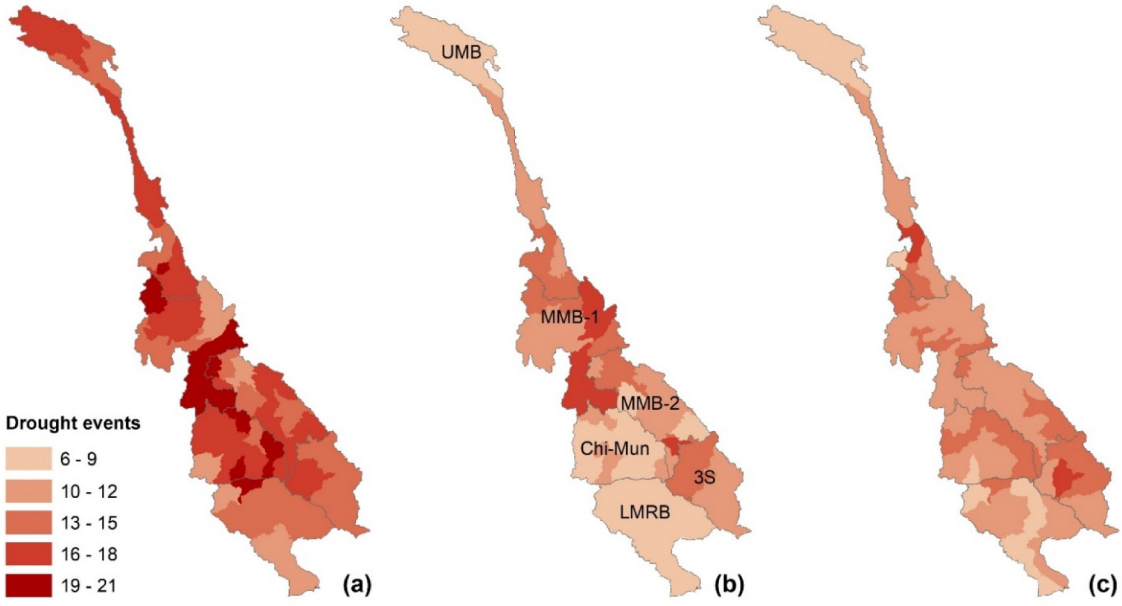

Fig. 7. Spatial distribution of drought events identified by (a) SPI, (b) SSWI, and (c) SRI over the Mekong River Basin.

Table 5
The number of average drought events in six main subbasins.

	UMB	MMB-1	MMB-2	Chi-Mun	3S	LMRB
SPI	16	18	16	17	15	13
SSWI	8	13	12	9	13	8
SRI	9	12	12	12	13	11

Table 6
Number of drought frequency (%) on average identified by different droughts in six main subbasins.

	UMB	MMB-1	MMB-2	Chi-Mun	3S	LMRB
SPI	16	15	16	15	15	13
SSWI	17	15	15	13	16	11
SRI	17	16	16	15	16	15

4.3.2. Drought frequency

Spatial distributions of drought frequency over the MRB are shown in Fig. 8. Overall spatial patterns of drought frequency were less distinct than those of drought events shown in Fig. 7. Most MRB was covered by drought frequency higher than the range of 13 % to 15 % for all types of droughts, and the downstream basins had a lower frequency than the upstream basins. Only the SSWI and SRI observed drought frequency larger than 19 % showing the impact of prolonged meteorological droughts often lasting longer for developing agricultural and hydrological droughts. Table 6 shows the average frequency in six main subbasins. Differences in averaged drought frequency calculated by SPI, SSWI, and SRI were not significant, only the SRI was 4 % and 2 % larger than that of SSWI and SPI, respectively, in the LMRB. During drought events, low streamflow months lasted longer due to dense populations and irrigations in the LMRB.

4.3.3. Drought severity

Drought severity calculated by SPI, SSWI, and SRI is shown in Fig. 9. Spatial variations in both SSWI and SRI values were more distinct than those in SPI. Drought severity in the UMB was worse than those in the lower basins for both SSWI and SRI, while the SPI values were similar throughout the entire MRB. Table 7 shows the averaged drought severity in the six main subbasins. The UMB had the worst severity in all three indices, while the SSWI was less severe than both SPI and SRI in the other five main subbasins. The drought severity of Chi-Mun and LMRB had the smallest SSWI values among all subbasins which can be explained by fewer drought events identified in those two subbasins as shown in Table 5. On the other hand, fewer SSWI drought events with the worst severity were observed in the UMB. It can be explained by the lower water holding capacity and steeper terrain in the UMB than those in the Chi-Mun and LMRB.

4.3.4. Differences in drought characteristics between the UMB and LMRB

Drought in the MRB often induced severe food security problems and affected socio-economic activities. Differences in drought characteristics between the most upstream basin (i.e., UMB) and the most downstream basin (i.e., LMRB) are compared as shown in Fig. 10. Overall, more drought events, higher frequencies, and severity were observed in the UMB than those in the LMRB, except for the SSWI and SRI events. Particularly, the agricultural and hydrological droughts were more intensified in the UMB with a severity value of −124 for both types of droughts than those in the LMRB with values of −88 and −105, respectively. Differences in the SPI severity between these two subbasins were much less than those in SSWI and SRI severities. Table 8 shows the event-averaged drought severity calculated as the drought severity divided by the number of drought events. Averaged SPI severity in the UMB and the LMRB were −7 and −8, respectively. Similar averaged SPI severity meant normalized reductions in precipitation were comparable between the most upstream and the most downstream subbasins. However, the shortage of precipitation amount during SPI drought events in the LMRB was often more substantial than that in the UMB, which may induce greater impacts on the LMRB as extended socio-economic and agricultural activities in the area. On the other hand, averaged SSWI and SRI severity in the UMB were more intensified than those in the LMRB, it can be explained by distinct basin characteristics between the most upstream and downstream subbasins. The UMB is a mountainous basin with steep topography, sandy loam soils, and grassland-dominated land cover. Such basin characteristics contribute lower water holding capacity and faster runoff generation than those of the LMRB. Reductions in soil moisture and discharges were more significant in the upstream basins. Therefore, the UMB was more vulnerable to severe agricultural and hydrological droughts than the LMRB.

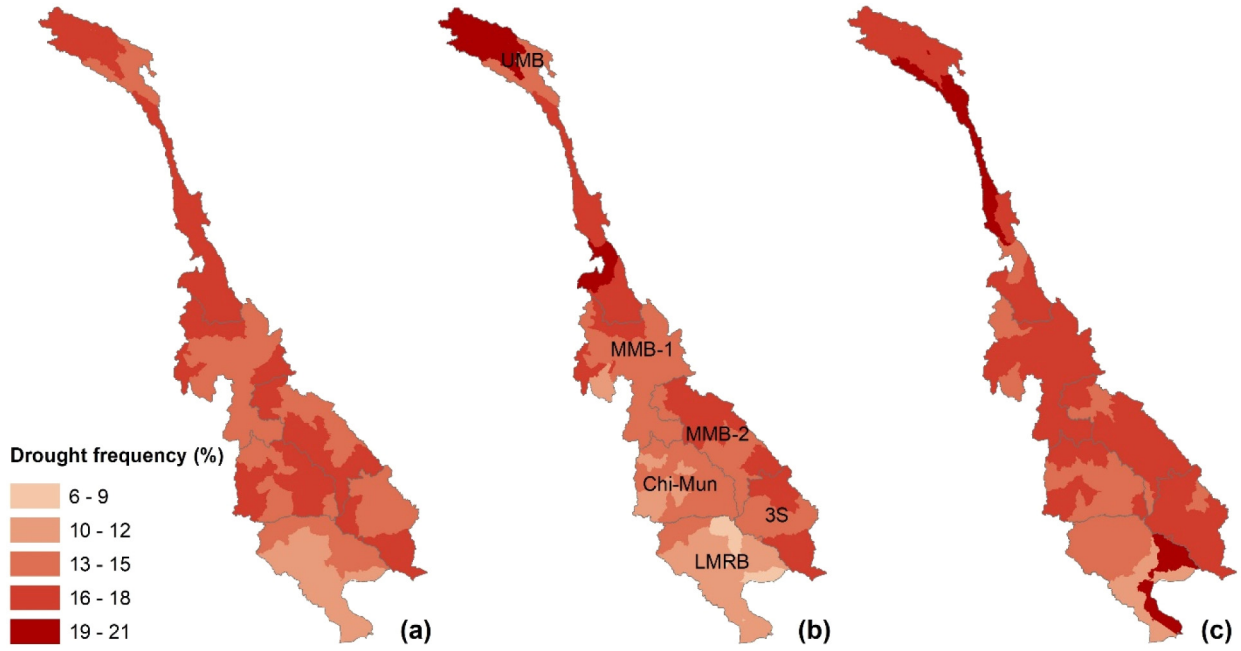

Fig. 8. Drought frequency (%) identified by (a) SPI, (b) SSWI, and (c) SRI over the Mekong River Basin.

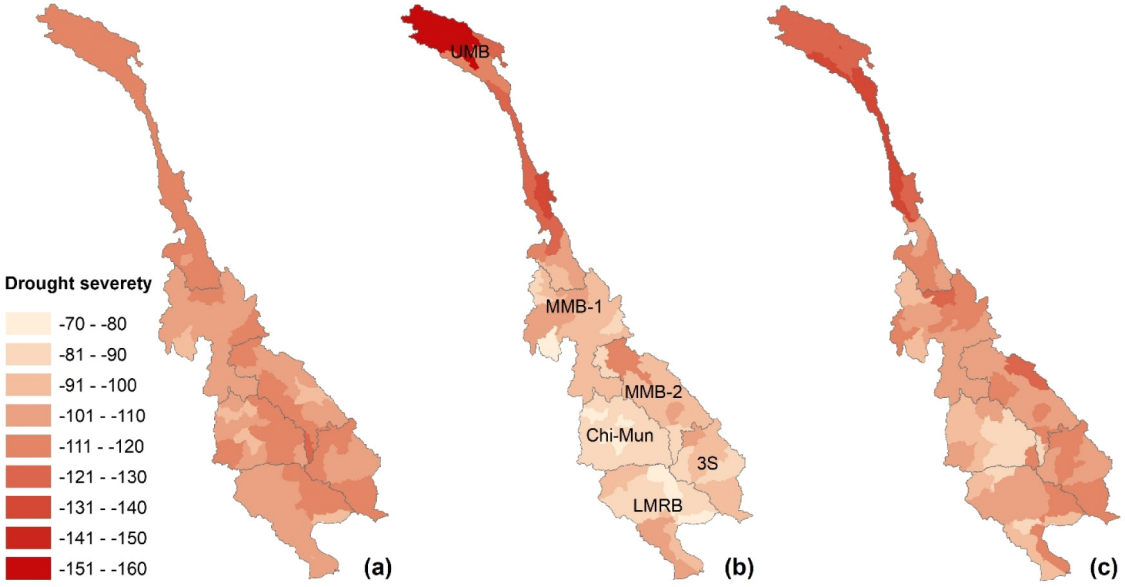

Fig. 9. Drought severity identified by (a) SPI, (b) SSWI, and (c) SRI over the Mekong River Basin.

4.4. Spatiotemporal variations in teleconnection with ENSO

4.4.1. Teleconnection between ENSO and precipitation, soil water content, and discharge

The years of El Niño between 1970 and 2007, including 1972–1973, 1976–1977, 1979–1980, 1982–1983, 1986–1987, 1991–1992, 1994–1995, 1997–1998, 2002–2003, 2004–2005, 2006–2007, were adopted from the Climate Prediction Center (CPC) for teleconnection analysis in this study. Anomalies of annual precipitation, soil water content, and discharge in six main subbasins during El Niño years are shown in Fig. 11. The median values of anomalies in all three variables were negative throughout the MRB, indicating reduced precipitation, soil water content, and discharge during most El Niño years. Deviations in anomalies of precipitation and soil water content were smaller than that in the discharge. Larger negative anomalies were observed in the southern MRB than those in the northern MRB for all three variables. For example, the most negative anomalies in precipitation were found in 3S and LMRB with relatively smaller deviations in anomaly values which meant different ENSO years consistently contributed to reduced precipitation. For anomalies in soil water content, differences in median values and deviations among subbasins were smaller than those observed in precipitation and discharge. For example, the median values of anomalies in MMB-1, MMB-2, Chi-Mun, 3S, and LMRB were close to each other except that in the UMB. However, deviations in anomalies of discharge were more significant than those in precipitation and soil water content. The median values of anomalies in discharge were smaller than −10 % in MMB-2, Chi-Mun, 3S, and LMRB with large deviations.

Table 7
Averaged drought severity identified by SPI, SSWI, and SRI in six main subbasins.

	UMB	MMB-1	MMB-2	Chi-Mun	3S	LMRB
SPI	−113	−107	−110	−107	−112	−106
SSWI	−124	−96	−98	−83	−96	−88
SRI	−124	−106	−106	−96	−112	−105

The LMRB is a globally renowned transnational basin with rice productivity and biodiversity. The temporal correlations of anomalies in precipitation, soil water content, and discharge with ENSO in this region are examined in Fig. 12. The negative hydrological variations were found to be associated with the strongest El Niño events between 1970 and 2007. Significant reductions in precipitations were observed in five ENSO events. Particularly, large precipitation variations (< −10 %) were observed in ENSO years, for instance 1992 and 1998 were recorded as the extreme drought years in the MRB (Prapertchob et al., 2007; Nguyen and Shaw,

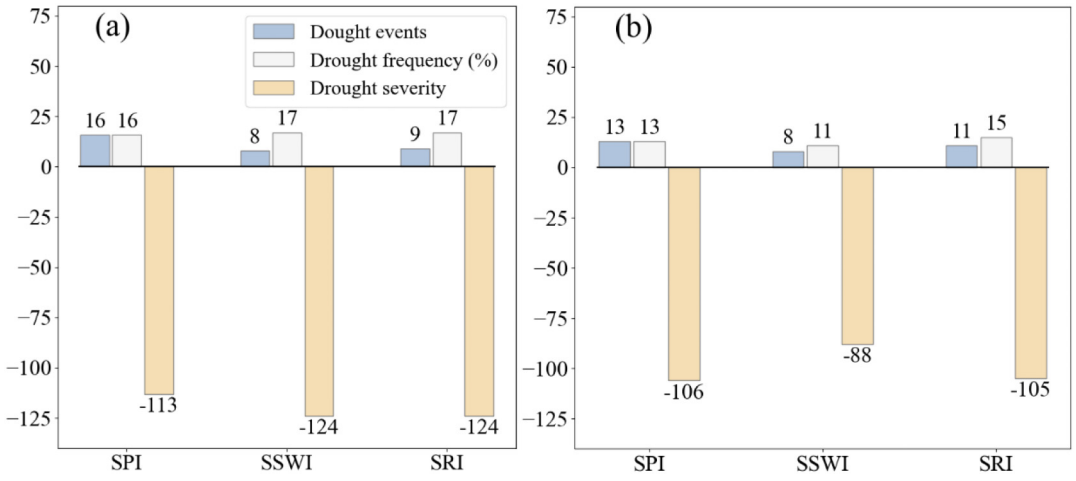

Fig. 10. Differences in drought events, frequency, and severity between (a) the UMB and (b) the LMRB.

Table 8
Event-averaged drought severity in the UMB and LMRB.

	UMB	LMRB
SPI	−7	−8
SSWI	−16	−11
SRI	−14	−10

2011). In addition, reductions in soil water content and discharge were found in all six ENSO events. Notably, soil water content anomalies in 1972 and 1986 and discharge anomalies in 1987 and 1998 were associated with ENSO years, with reductions of more than −25 %. Although the year 1993 wasn't classified as an ENSO year, a reduction of 20 % in precipitation was seen with a positive ENSO index value. The occurrences of negative hydrological variations, mostly coincided with the mature phase of El Niño showing the reduction of precipitation, soil water content, and discharge in the dry months related to the strong ENSO events.

Fig. 13 shows the spatial distribution of the Pearson correlation coefficient between ENSO and precipitation, soil water content, and discharge. The negative correlation values indicated reduced precipitation, soil water content, and discharge during the El Niño events, and most of the MRB showed insignificant correlations with respect to the ENSO events. Areas having less significant ENSO correlations were masked in white color for clarity. It can be observed that the correlations between ENSO and precipitation were mainly found in the southern MRB, while the correlations between ENSO and soil water content were scattered over the middle to the southern MRB. Since the entire MRB has latitudes roughly from 10°N to 35°N (Fig. 1), which encompasses high-altitude continental and temperate in the upper basin to tropical monsoonal in the lower basin. In addition to the ENSO effects, the precipitation in the middle and lower MRB is mainly dominated by the East Asia-Western North Pacific monsoon and the Indian monsoon with different spatial extents (Delgado et al., 2012). Although the spatiotemporal influences of Asia monsoons in the MRB are quite heterogeneous, the development of the East Asia monsoon is also affected by the ENSO. Unlike the lower MRB with integrated effects of ENSO and the East Asia monsoon, the ENSO correlation in the upper MRB is insignificant partly due to its high-altitude continental and temperate climate. As a result, the less significant ENSO correlation was masked in white color as shown in Fig. 13. The ENSO correlations with discharge and soil water content were observed less significant than that of ENSO with precipitation. The ENSO effects on discharge and soil water content are modulated by basin hydrological processes and become less significant due to longer residence time in surface water and soil water than that in atmospheric water. Finally, the correlations between ENSO and discharge were only situated in the southeastern parts. Table 9 presents averaged correlations between ENSO and all three variables. The ENSO index values in DJF months provide a high potential for hydrological outlooks in MAM months of precipitation and in AMJ months for both soil water content and discharge. The 3S and LMRB had significant correlations values ranging between −0.5 and −0.67 ($p < 0.05$), while the UMB and MMB-1 had insignificant correlations values larger than −0.5. Besides, ENSO correlation with precipitation was more significant than with soil water content and discharge in all subbasins. Precipitation variations were more sensitive to the development of ENSO events, which may further affect changes in soil water and river discharge in addition to the effects of agricultural practices and water resources management.

4.4.2. Teleconnection between ENSO and multiple drought indices

Great reduction in hydrological quantities often induced droughts in the MRB. The previous section showed negative anomalies in precipitation, soil water content, and discharge were highly correlated with the ENSO events. How the ENSO events related to different types of droughts were presented as the spatial correlation between ENSO and three drought indices (i.e., SPI, SSWI, and SRI) in six main subbasins in Fig. 14. Areas having less significant ENSO correlations were also masked in white color for clarity in the figure. It can be seen that the correlation between ENSO and SPI was observed in most of the southern MRB while the major influences of ENSO on SSWI and SRI were only found in the LMRB and 3S, respectively. Similar to the overall pattern as shown in Fig. 13 but having local differences, the overall ENSO correlation with drought indices showed higher correlations in the lower basins and lower correlations in the upper basins. Table 10 presents the correlation values between ENSO and three drought indices. It is noticeable that significant negative correlations between ENSO and drought indices were found in the southern MRB. Particularly, the ENSO had a strong connection to meteorological droughts in the MMB-2, Chi-Mun, 3S, and LMRB, whereas the linkage between ENSO and droughts was not seen in the UMB and MMB-1. Both agricultural and hydrological droughts had strong connections with ENSO in the 3S and LMRB, but these correlations were not found in other regions. As shown in Table 10, ENSO had higher correlations with SPI than those with SSWI and SRI. The statistical analyses presented here suggest that the ENSO had a strong influence on droughts in the southern part, especially for meteorological droughts. The mature phase of ENSO in DJF months can be used as a precursor for watching the developments of meteorological droughts in MAM months and hydrological and agricultural droughts in AMJ months. Although drought indices were calculated by applying the standardization process to the precipitation, discharge, and soil water content, spatial differences in ENSO correlations between Figs. 13 and 14 were observed. According to the correlation values given in Tables 9 and 10, the changes in the averaged correlation values were quite different among different indices or subbasins. For example, increased correlations for the SPI and the SSWI and a decreased correlation for the SRI were observed in the 3S, but not seen in the other five subbasins. However, the decreased or increased correlations were insignificant for those having statistically significant values with $p < 0.05$.

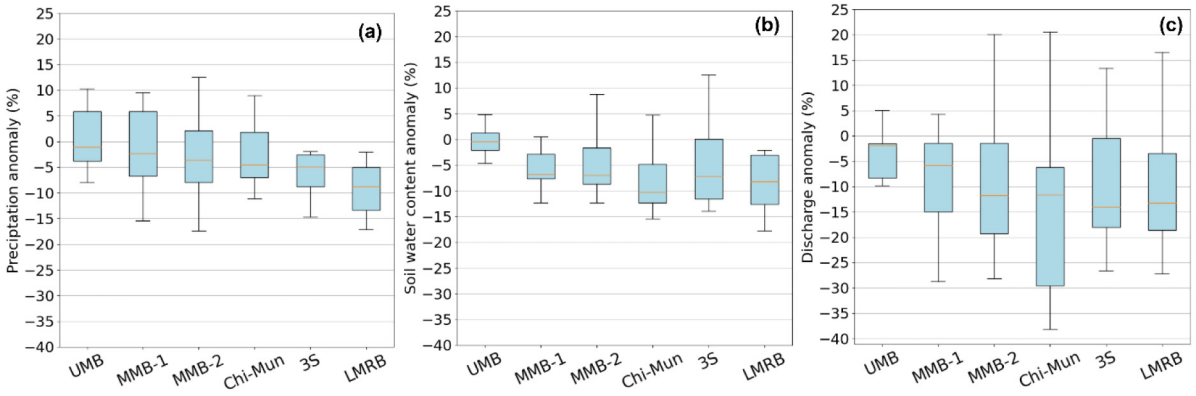

Fig. 11. (a) Precipitation, (b) soil water content, and (c) discharge anomalies during El Niño years of the period 1970–2007. The outer edges of the boxes represent the 25th and 75th percentiles, and the horizontal lines of the boxes represent the median.

5. Discussion

5.1. Spatial variability of soil water content

Spatial variability of soil water content is an important factor in spatial patterns of flood generation and agricultural activities for better farming and irrigation practices during droughts. Having larger variabilities of soil water content is often observed during the drying process due to the heterogeneity in vegetation, soil, and topography, while smaller variabilities are observed during the wetting process due to the wide area affected by heavy rainfalls. As a result, the relation between the coefficient of variation (CV) of spatial soil water content and mean spatial soil water content often shows such hysteresis patterns (Ivanov et al., 2010; Srivastava et al., 2021). To simplify the examination of whether the hysteresis pattern can be observed in this study, the CV of spatial soil water content in the UMB and LMRB during the extremely dry year 1992 was calculated as shown in Fig. 15. The CV values in the UMB were much larger than those in the LMRB. Similar to past studies observed, the drying process had larger variability than the wetting process. However, an increased CV trend was observed in the UMB during the wetting process, while a decreased CV trend was found in the LMRB. Distinct rainfall patterns dominated by the high-altitude continental and temperate climate in the UMB and the tropical monsoonal climate in the UMB might mainly account for such trend discrepancy in addition to differences in vegetation, soil, and topography between the UMB and the LMRB. However, further analyses are required to investigate which factors mainly contribute to such discrepancies in wetting trends.

The frequency distribution of soil water content during ENSO and non-ENSO years in the LMRB was presented in Fig. 16. The ENSO years were in 1972–1973, 1976–1977, 1979–1980, 1982–1983, 1986–1987, 1991–1992, 1994–1995, 1997–1998, 2002–2003, 2004–2005, and 2006–2007, as those shown in Fig. 12. The monthly soil water content values from April to June (i.e., the same months considered for ENSO-SSWI connections) were used to calculate the frequency of soil water content. There were significant differences in frequency distributions of soil water content between ENSO years and non-ENSO years. The ENSO years had larger (smaller) frequency values than the non-ENSO years for low (high) soil water content intervals. Differences in frequency values between the ENSO years and the non-ENSO years became larger for the intervals toward the higher and the lower soil water contents. Agricultural droughts in the LMRB (e.g., the SSWI in Fig. 14) during the ENSO years accounted for areas covered by drier soils that were broader than those during the non-ENSO years. On the contrary, the areas having wetter soils during the ENSO years were much less than those during the non-ENSO years.

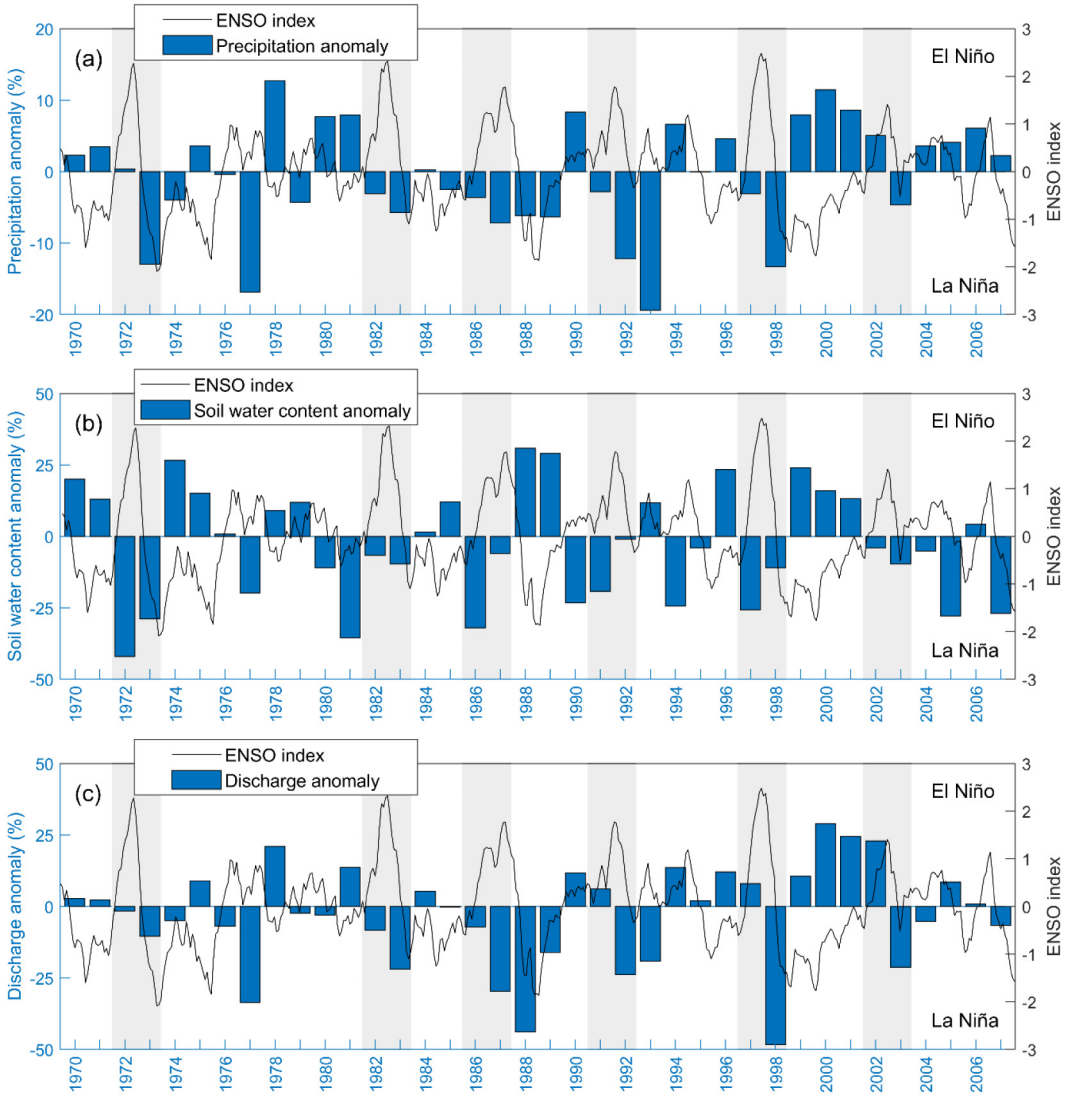

Fig. 12. Hydrological anomalies in the LMRB during the period 1970–2007, (a) precipitation anomaly, (b) soil water content anomaly, (c) discharge anomaly, and the monthly ENSO index. The grey columns indicate strong El Niño events (1972, 1982–1983, 1986–1987, 1991–1992, 1997–1998, 2002–2003).

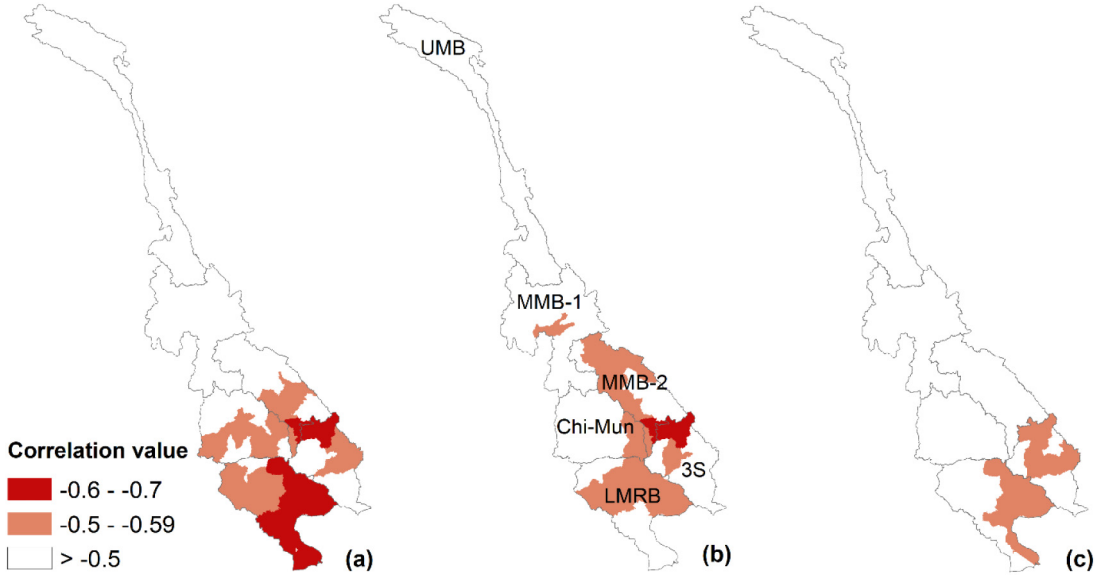

Fig. 13. Spatial Correlation between ENSO (DJF) and precipitation (MAM), soil water content/discharge (AMJ) presented at the 95 % confidence interval. (a) Precipitation, (b) soil water content, (c) discharge.

5.2. Comparison with other studies and ENSO-droughts relationships

Previous studies have assessed the historical droughts and indicated that severe droughts occurred in 1990–1992, 1997–1998, and 2005–2006 (Guo et al., 2017; Zhang et al., 2014; Kang and Sridhar, 2021; Lee and Dang, 2019; Liu, 2020; Palanisamy et al., 2021). Their results showed that the extreme droughts had significant impacts on the upper and lower MRB, especially in Thailand, Laos, Cambodia, and Vietnam. Moreover, Chi-Mun (Thailand) and the 3S (Vietnam) subbasins were more prone to droughts and very likely to have severe droughts in the future (Kang and Sridhar, 2021; Liu, 2020; Palanisamy et al., 2021; Thilakarathne and Sridhar, 2017). Similar results were observed in drought events identified in this study and shown in Table 5, the Chi-Mun had a larger SPI value and the 3S had larger SSWI and SRI values than both the MMB-2 and the LMRB had. Larger drought frequency and drought severity values were also observed for the 3S than those of the MMB-2, the Chi-Mun, and the LMRB subbasins (Tables 6 and 7).

The occurrences of strong El Niño events coincided with the appearance of severe droughts having larger negative anomalies in precipitation, soil water content, and discharge which were observed in the Chi-Mun, 3S, and LMRB as shown in Fig. 11. Meteorological droughts had more drought events and higher intensity than agricultural and hydrological droughts, as well as more sensitive to the ENSO than other types of droughts.

Table 9
Pearson's correlations and related *p*-value for correlation with ENSO (DJF) and precipitation (MAM), soil water content/discharge (AMJ) of six main subbasins (see the map of areas in Fig. 1). Statistically significant values with $p < 0.05$ are marked with one asterisk (*) and those with $p < 0.01$ with two asterisks (**).

	UMB	MMB-1	MMB-2	Chi-Mun	3S	LMRB
Precipitation	−0.27	−0.35	−0.58 **	−0.55**	−0.61**	−0.67**
Soil water content	−0.16	−0.44*	−0.57 *	−0.44*	−0.56**	−0.54**
Discharge	0.05	−0.23	−0.39*	−0.25	−0.5*	−0.55*

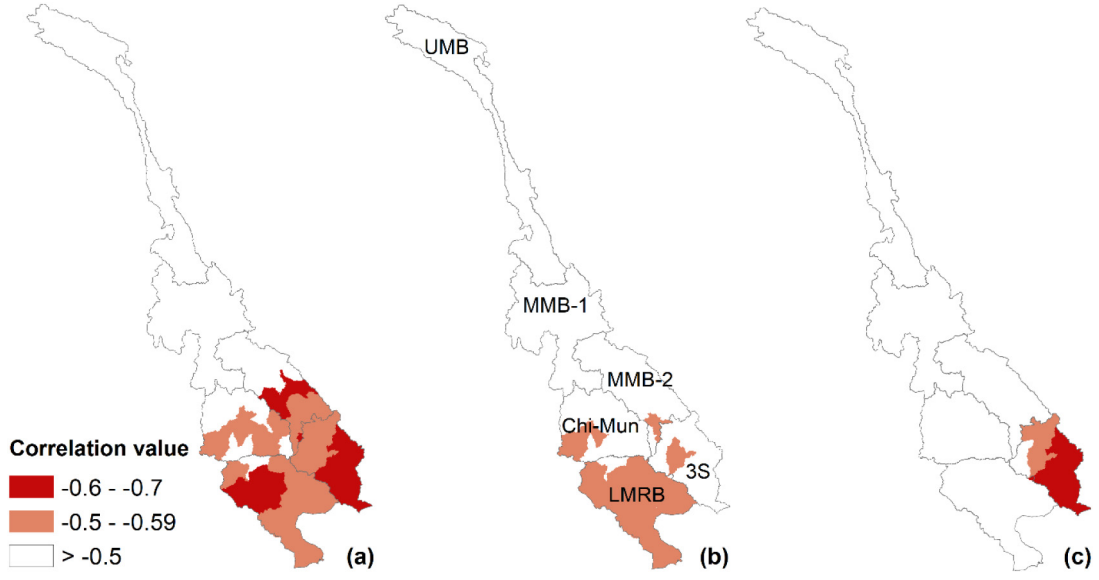

Fig. 14. The correlation between ENSO (DJF) and SPI (MAM), SSWI/SRI (AMJ) in different spatial presented at the 95 % confidence interval. (a) SPI, (b) SSWI, (c) SRI.

Table 10
Pearson's correlations and related *p*-value for correlation with ENSO (DJF) and SPI (MAM), and SSWI/SRI (AMJ) of six main subbasins (see the map of areas in Fig. 1). Statistically significant values with $p < 0.05$ are marked with one asterisk (*) and those with $p < 0.01$ with two asterisks (**).

	UMB	MMB-1	MMB-2	Chi-Mun	3S	LMRB
SPI	0.10	−0.12	−0.59**	−0.57**	−0.70**	−0.64**
SSWI	0.25	−0.25	−0.47*	−0.47*	−0.50**	−0.55**
SRI	0.04	−0.18	−0.37*	−0.29	−0.65**	−0.47*

Precipitation is one of the key variables driving various hydrological processes while discharge and soil water content are controlled in part by antecedent precipitation with higher residence time that modulated the forcing of precipitation variability (Xue et al., 2011). As a result, the correlation between ENSO and hydrological droughts was more significant than the correlation between ENSO and hydrological/agricultural droughts (Räsänen and Kummu, 2013; Xu et al., 2004; Xue et al., 2011).

The LMRB had high correlations with ENSO, especially in meteorological drought as presented in studies by Räsänen and Kummu (2013), Räsänen et al. (2016), and Xue et al. (2011). This shows a potential implication for drought outlooks which are very likely applicable to adopting the lead-time connections between ENSO and droughts as the results shown in Section 4.4. In this study, we have strengthened the understanding of drought characteristics in the MRB; including (1) distinct drought severity between the UMB and LMRB and (2) the highest correlation between meteorological drought and ENSO was observed in the 3S basin with a value of −0.7. The 3S basin was documented as large drought-prone in the MRB and recorded with noticeable impacts by extreme drought events (Nguyen and Shaw, 2011; Vu et al., 2015b). In addition to ENSO events, a variety of East Asian monsoons also played an important role to affect the climate and weather in the MRB. For example, the extreme precipitation variability across the MRB was most significantly correlated with the East Asian Summer Monsoon (Irannezhad et al., 2022). Climate variabilities in the northern MRB are mainly affected by variations in the Indian monsoon (Bansod et al., 2003; Kripalani and Kulkarni, 1997), while the southern MRB is sensitive to the East Asian monsoon (Xue et al., 2011). The influences of ENSO on the downstream basin may become more significant as more dams are being constructed in the next few decades (Xue et al., 2011). The results of this study would contribute to an enormous potential for a drought early warning system based on the ENSO large-scale index, especially in the southern part of the basin. For the northern part of MRB, there is no correlation with ENSO, thus it is possible to consider the teleconnections with other climate indices, such as the Pacific Decadal Oscillation or Indian Ocean Dipole, which are known to influence rainfall during different seasonal periods. Particularly, we can adopt ENSO in DJF months as a precursor to observe the onset of meteorological drought in MAM and hydrological drought in AMJ months. The results are of great societal impacts in improving the possibility of developing drought watch against extreme droughts to enhance the sustainability of water resources in the basin.

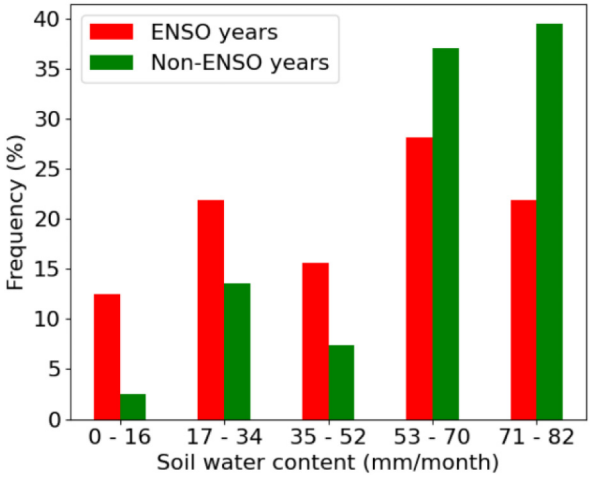

Fig. 16. The frequency distribution of soil water content for the ENSO years and none-ENSO years in the LMRB.

5.3. Uncertainties and limitations

The uncertainties of the SPI might result from limited record length, trends, and outliers (Carbone et al., 2018; Vergni et al., 2017; Zhang and Li, 2020). At least 30 years of continuous data are required to calculate the SPI as suggested in a study by McKee et al. (1993). Carbone et al. (2018) indicated that the SPI derived from the 30-year record has considerably more uncertainty than those from the 60-year record based on a study using 14 Italian stations. In this study, only 38 years of data from 1970 to 2007 were considered to calculate drought indices and should be improved by collecting more data in a future study, such as to include drought events that occurred after 2010 (e.g., 2016 and 2019–2020) in the MRB. The selection of different accumulation periods for calculating drought indices may also induce uncertainties. In this study, the accumulation period of 6 months was used by considering not using longer accumulation periods (e.g., 12 months) that might dissimulate differences among indices and shorter accumulation periods (e.g., 3 months) that might induce large discrepancies such as the drought only occurred as a meteorological event. It is thus suggested to examine the uncertainty in association with using the different accumulation time periods in future studies.

Since the hydrological simulations were adopted to provide discharge and soil water content data for calculating hydrological and agricultural drought indices, the uncertainty in association with the model selected and the input data for hydrological simulations was addressed herein. In addition to the SWAT model used in this study, the Variable Infiltration

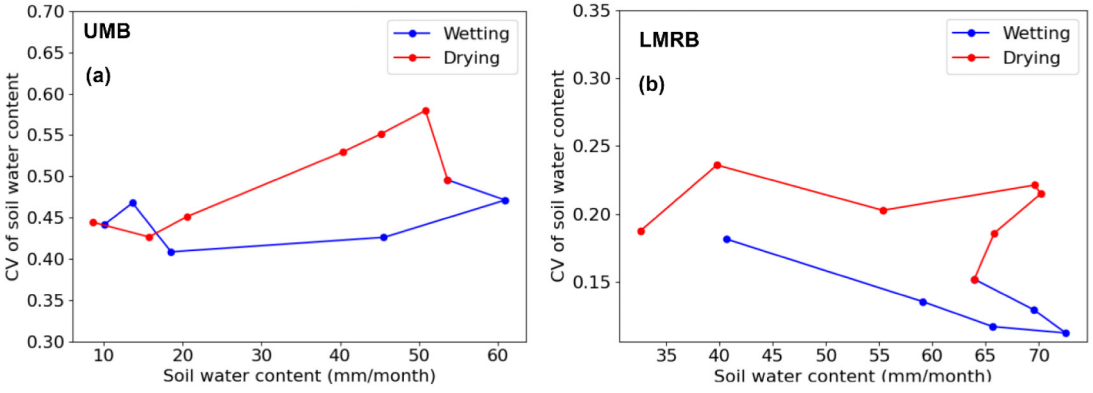

Fig. 15. The relationship between CV of soil water content and mean soil water content in (a) the UMB and (b) the LMRB in 1992.

Capacity (VIC) models have been applied to study droughts in the MRB (Kang and Sridhar, 2021; Zhang et al., 2020; Thilakarathne and Sridhar, 2017). Although how to simulate hydrological processes is quite model-dependent, calibration and validation processes were often employed to ensure model performance is acceptable and to minimize model errors. Performing model-intercomparisons by using different hydrological models with the same input data sets and simulation settings is suggested to resolve the uncertainty in association with the hydrological model selected. Other issues related to hydrological simulations are input data sets and simulation settings. For example, the gridded precipitation data, the land use data, and the soil data may contribute to the uncertainty in terms of their spatial and temporal resolutions (i.e., part of the simulation setting) used for hydrological simulations. In this study, the land use data were obtained from the GLCC dataset by using the same setting for long-term hydrological simulations. It is suggested to build different SWAT models in association with reliable time-varying land use data for each sub-period simulation. Finally, a total of 87 subbasins with 983 hydrological response units were used for the SWAT simulations in this study. Spatial resolutions are often another concerning source of uncertainty. Finer spatial resolutions are suggested whenever the detailed spatial variability is expected to be investigated, yet it is also subject to the availability of the input data. It is the limitation in this study of not performing different spatial resolution tests to determine the best size of subbasins. However, calibration and validation results demonstrated that our hydrological simulations were acceptable to provide reliable hydrological variables for drought assessments.

6. Conclusions

This study investigated the spatiotemporal aspects of multiple droughts (i.e., meteorological, agricultural, and hydrological droughts) in the MRB and their relationship with the ENSO index. Results from our assessment highlighted the drought-prone areas in the MRB and showed spatial variations in drought characteristics in the entire MRB, especially differences in drought severity between the UMB and LMRB. Furthermore, the findings provided more comprehensive information on the linkages between ENSO and droughts in this large watershed. In particular, meteorological drought has identified more events with a higher intensity than agricultural and hydrological droughts, while a higher frequency has been observed in hydrological drought. The middle Mekong basins were observed with a higher number of drought occurrences while the UMB had higher drought frequency and intensity. A strong connection between ENSO (DJF) and SPI (MAM), and SSWI/SRI (AMJ) was found in the southern part of MRB, but there were insignificant correlations in the northern part of the MRB. Thus, the development of ENSO in DJF months can be used as a precursor to observing the developments of meteorological drought in MAM months and hydrological and agricultural droughts in AMJ months in the most downstream of the MRB (e.g., 3S and LMRB). Droughts are projected to have detrimental impacts on agriculture, fishery, and ecosystems in the LMRB, especially in the context of rapid developments, thus calling for timely mitigation and adaptation to cope with extreme drought events. These results have great potential for predicting droughts based on ENSO-drought linkages and are useful to support development planning and strategic decision-making in the MRB.

CRediT authorship contribution statement

Thi-Thu-Ha Nguyen: Conceptualization, Methodology, Data curation, Software, Writing-original draft. Ming-Hsu Li: Conceptualization, Supervision, Funding acquisition, Writing-review & editing. Minh-Tue Vu: Conceptualization, Data curation, Writing-review & editing. Pei-Yuan Chen: Review & editing.

Data availability

Precipitation and air temperature data were retrieved from APHRODITE and CPC datasets, available at http://aphrodite.st.hirosaki-u.ac.jp/products.html and https://www.cpc.ncep.noaa.gov, respectively. The GTOPO30 from the United States Geological Survey is a global digital elevation model having a horizontal grid spacing of 30 arc *sec* (roughly 1 km), it is available at https://earthexplorer.usgs.gov/. Land use and land cover data were obtained from the European Commission at https://forobs.jrc.ec.europa.eu/products/glc2000/products.php. Soil data were from the Harmonized World Soil Database (HWSD) (http://www.fao.org/soils-portal/soil-survey/soil-maps-and-databases/harmonized-world-soil-database-v12/en/) from the Food and Agriculture Organization of the United Nations. The ONI of region 3.4 is available from the website of NOAA (https://www.cpc.ncep.noaa.gov/). The daily discharge data at mainstream stations were obtained by the authors from the Mekong River Commission (https://portal.mrcmekong.org/home). All these data are publicly available and were accessed in Dec. 2020.

Declaration of competing interest

The authors declare that they have no known competing financial interests or personal relationships that could have appeared to influence the work reported in this paper.

Acknowledgments

This study was supported by the Ministry of Science and Technology, Taiwan, under Contract No. MOST-107-2116-M-008-002 and MOST-108-2116-M-008-003 with the National Central University. We would like to thank Dr. Thanh Duc Dang and Dr. Duong Anh Tran for their meaningful support and suggestions on this work.

Appendix A. Sensitive analysis

In this study, 15 parameters were selected for sensitive analysis by evaluating their *p*-value (Abbaspour et al., 2007). A low *p*-value (≤ 0.05) indicates that the null hypothesis can be rejected. The predictor having low value is likely to be a meaningful addition to the model because changes in the predictor's value are related to changes in the response variable. A higher *p*-value, on the other hand, indicates that there is no association with changes in the response. With a *p*-value of 0.05, there is only a 5 % chance that the results would have come up in a random distribution, and can be concluded that the variable is having an effect with a 95 % confidence level. In SUFI-2, the methods for adjusting the parameter values are denoted by the first letter before the parameter name (R, V, and A). The letter V denotes replacing the current parameter value. The letter A denotes adding a given value to the current parameter value, and the letter R denotes multiplying (1 + a given value) to the current parameter value. All 15 parameters present in Table A1 were chosen based on previous studies in the MRB (Kang and Sridhar, 2021; Kang et al., 2021). There were eight parameters (i.e., CN2, GW-REVAP, ALPHA_BF, CH_K2, SOL_K, CH_N2, GW_DELAY, ESCO), which were the most dominant parameters that should be considered for calibration.

Table A1
The sensitive analysis results.

No.	Parameters	*P*-value
1	R_CN2.mgt	0.00004
2	V_GW_REVAP.gw	0.00071
3	V_ALPHA_BF.gw	0.00122
4	V_CH_K2.rte	0.00486
5	R_SOL_K(..).sol	0.00679
6	V_CH_N2.rte	0.01256
7	V_GW_DELAY.gw	0.02541
8	V_ESCO.bsn	0.04862
9	V_GWQMN.gw	0.38439
10	r_SOL_AWC(1).sol	0.47024
11	V_SOL_K(1).sol	0.60962
12	V_SOL_BD(1).sol	0.78520
13	V_SFTMP.bsn	0.85614
14	V_ALPHA_BNK.rte	0.94102
15	V_CH_N2.rte	0.94129

References

Abbaspour, K.C., Johnson, C., Van Genuchten, M.T., 2004. Estimating uncertain flow and transport parameters using a sequential uncertainty fitting procedure. Vadose Zone J. 3, 1340–1352.

Abbaspour, K.C., Vejdani, M., Haghighat, S., Yang, J., 2007. SWAT-CUP calibration and uncertainty programs for SWAT. MODSIM2007 International Congress on Modeling and Simulation, Modeling and SimulationSociety of Australia and New Zealand. Swiss Federal Institute of Aquatic Science and Technology Dübendorf, Switzerland, pp. 1596–1602.

Abhishek, A., Das, N.N., Ines, A.V., Andreadis, K.M., Jayasinghe, S., Granger, S., Ellenburg, W.L., Dutta, R., Quyen, N.H., Markert, A.M., et al., 2021. Evaluating the impacts of drought on rice productivity over Cambodia in the lower Mekong basin. J. Hydrol. 599, 126291.

Arnold, J.G., Srinivasan, R., Muttiah, R.S., Williams, J.R., 1998. Large area hydrologic modeling and assessment part i: model development 1. J. Am. Water Resour. Assoc. 34, 73–89.

Arnold, J.G., Moriasi, D.N., Gassman, P.W., Abbaspour, K.C., White, M.J., Srinivasan, R., Santhi, C., Harmel, R., Van Griensven, A., Van Liew, M.W., et al., 2012. SWAT: model use, calibration, and validation. Trans. ASABE 55, 1491–1508.

Bansod, S.D., Yin, Z.-Y., Lin, Z., Zhang, X., 2003. Thermal field over Tibetan plateau and Indian summer monsoon rainfall. Int. J. Climatol. 23, 1589–1605.

Carbone, G.J., Lu, J., Brunetti, M., 2018. Estimating uncertainty associated with the standardized precipitation index. Int. J. Climatol. 38, e607–e616.

Chu, T.H., Hans, G., Peter, D., Jeroen, A., 2003. Water, climate, food, and environment in the Mekong basin in southeast Asia. Technical Report. Mekong River Commission.

Cosslett, T.L., Cosslett, P.D., 2018. The lower Mekong basin: rice production, climate change, ENSO, and Mekong dams. Sustainable Development of Rice and Water Resources in Mainland Southeast Asia and Mekong River Basin. Springer, pp. 85–114.

Cunderlik, J., 2003. *Hydrologic model selection for the CFCAS project: Assessment of water resources risk and vulnerability to changing climatic conditions*. The University of Western Ontario, Canada.

Dang, T.D., Chowdhury, A., Galelli, S., 2020. On the representation of water reservoir storage and operations in large-scale hydrological models: implications on model parameterization and climate change impact assessments. Hydrol. Earth Syst. Sci. 24, 397–416.

Davey, M., Brookshaw, A., Ineson, S., 2014. The probability of the impact of ENSO on precipitation and near-surface temperature. Clim. Risk Manag. 1, 5–24.

Delgado, J.M., Merz, B., Apel, H., 2012. A climate-flood link for the lower Mekong River. Hydrol. Earth Syst. Sci. 16, 1533–1541.

Dong, Z., Liu, H., Hu, H., Khan, M.Y.A., Wen, J., Chen, L., Tian, F., et al., 2022. Future projection of seasonal drought characteristics using CMIP6 in the Lancang-Mekong river basin. J. Hydrol. 610, 127815.

Fok, H.S., He, Q., Chun, K.P., Zhou, Z., Chu, T., 2018. Application of ENSO and drought indices for water level reconstruction and prediction: a case study in the lower Mekong river estuary. Water 10, 58.

Guo, H., Bao, A., Liu, T., Ndayisaba, F., He, D., Kurban, A., De Maeyer, P., 2017. Meteorological drought analysis in the lower Mekong Basin using satellite-based long-term CHIRPS product. Sustainability 9, 901.

Guttman, N.B., 1999. Accepting the standardized precipitation index: a calculation algorithm 1. J. Am. Water Resour. Assoc. 35, 311–322.

Hoang, L.P., Lauri, H., Kummu, M., Koponen, J., Van Vliet, M.T., Supit, I., Leemans, R., Kabat, P., Ludwig, F., 2016. Mekong river flow and hydrological extremes under climate change. Hydrol. Earth Syst. Sci. 20, 3027–3041.

Irannezhad, M., Liu, J., Chen, D., 2022. Extreme precipitation variability across the lancang-Mekong river basin during 1952–2015 in relation to teleconnections and summer monsoons. Int. J. Climatol. 42, 2614–2638.

Ivanov, V.Y., Fatichi, S., Jenerette, G.D., Espeleta, J.F., Troch, P.A., Huxman, T.E., 2010. Hysteresis of soil moisture spatial heterogeneity and the "homogenizing" effect of vegetation. Water Resour. Res. 46, 1–15.

Kang, H., Sridhar, V., 2021. A near-term drought assessment using hydrological and climate forecasting in the Mekong river basin. Int. J. Climatol. 41, E2497–E2516.

Kang, H., Sridhar, V., Mainuddin, M., Trung, L.D., 2021. Future rice farming threatened by drought in the lower Mekong Basin. Sci. Rep. 11 (1), 1–15.

Kang, H., Sridhar, V., Ali, S.A., 2022. Climate change impacts on conventional and flash droughts in the Mekong river basin. Sci. Total Environ., p. 155845

Keovilignavong, O., Nguyen, T.H., Hirsch, P., 2021. Reviewing the causes of Mekong drought before and during 2019–20. Int. J. Water Resour. Dev. 1–21.

Kiem, A.S., Geogievsky, M.V., Hapuarachchi, H.P., Ishidaira, H., Takeuchi, K., 2005. RelationshipBetween ENSO and Snow Covered Area in the Mekong and Yellow River Basins. IAHS-AISH publication, pp. 255–264.

Kingston, D., Thompson, J.R., Kite, G., 2011. Uncertainty in climate change projections of discharge for the Mekong river basin. Hydrol. Earth Syst. Sci. 15, 1459–1471.

Konapala, G., Mishra, A.K., Wada, Y., Mann, M.E., 2020. Climate change will affect global water availability through compounding changes in seasonal precipitation and evaporation. Nat. Commun. 11, 1–10.

Kripalani, R.H., Kulkarni, A., 1997. Rainfall variability over south-East Asia - connections with indian monsoon and ENSO extremes: new perspectives. Int. J. Climatol. 17, 1155–1168.

Krysanova, V., White, M., 2015. Advances in water resources assessment with SWAT - an overview. Hydrol. Sci. J. 60, 771–783.

Kumari, N., Srivastava, A., Sahoo, B., Raghuwanshi, N.S., Bretreger, D., 2021. Identification of suitable hydrological models for streamflow assessment in the kangsabati river basin, India, by using different model selection scores. Nat. Resour. Res. 30, 4187–4205.

Lauri, H., de Moel, H., Ward, P.J., Keskinen, M., Kummu, M., 2012. Future changes in Mekong river hydrology: impact of climate change and reservoir operation on discharge. Hydrology and Earth System Sciences 16, 4603–4619.

Lauri, H., Räsänen, T., Kummu, M., 2014. Using reanalysis and remotely sensed temperature and precipitation data for hydrological modeling in monsoon climate: Mekong River case study. J. Hydrometeorol. 15, 1532–1545.

Lee, S.K., Dang, T.A., 2019. Spatio-temporal variations in meteorology drought over the Mekong River Delta of Vietnam in the recent decades. Paddy Water Environ. 17, 35–44.

Leng, G., Tang, Q., Rayburg, S., 2015. Climate change impacts on meteorological, agricultural and hydrological droughts in China. Glob. Planet. Chang. 126, 23–34.

Li, M., Di, Z., Duan, Q., 2021a. Effect of sensitivity analysis on parameter optimization: case study based on streamflow simulations using the SWAT model in China. J. Hydrol. 603, 126896.

Li, Y., Lu, H., Yang, K., Wang, W., Tang, Q., Khem, S., Yang, F., Huang, Y., 2021b. Meteorological and hydrological droughts in Mekong river basin and surrounding areas under climate change. J. Hydrol.: Reg. Stud. 36, 100873.

Liang, X., Lettenmaier, D.P., Wood, E.F., Burges, S.J., 1994. A simple hydrologically based model of land surface water and energy fluxes for general circulation models. J. Geophys. Res. 99 (D7), 14415–14428. https://doi.org/10.1029/94JD00483.

Liu, H., 2020. Flood Prevention and Drought Relief in Mekong River Basin. Springer.

Loc, H.H., Van Binh, D., Park, E., Shrestha, S., Dung, T.D., Son, V.H., Truc, N.H.T., Mai, N.P., Seijger, C., 2021. Intensifying saline water intrusion and drought in the Mekong delta: from physical evidence to policy outlooks. Sci. Total Environ. 757, 143919.

Lu, X.X., Chua, S.D.X., 2021. River discharge and water level changes in the Mekong river: droughts in an era of mega-dams. Hydrol. Process. 35, e14265.

McKee, T.B., Doesken, N.J., Kleist, J., et al., 1993. The relationship of drought frequency and duration to time scales. Proceedings of the 8th Conference on Applied Climatology. 17, pp. 179–183 California.

Mekong River Commission, 2005. Overview of the hydrology of the Mekong Basin. Mekong River Commission, Vientiane, p. 82.

Mondal, S.K., Huang, J., Wang, Y., Su, B., Zhai, J., Tao, H., Wang, G., Fischer, T., Wen, S., Jiang, T., 2021. Doubling of the population exposed to drought over South Asia: CMIP6 multi-model-based analysis. Sci. Total Environ. 771, 145186.

Moriasi, D.N., Arnold, J.G., Van Liew, M.W., Bingner, R.L., Harmel, R.D., Veith, T.L., 2007. Model evaluation guidelines for systematic quantification of accuracy in watershed simulations. Trans. ASABE 50, 885–900.

Nash, J.E., Sutcliffe, J.V., 1970. River flow forecasting through conceptual models part I - a discussion of principles. J. Hydrol. 10, 282–290.

Nguyen, H., Shaw, R., 2011. Adaptation to droughts in Cambodia. Droughts in Asian monsoon region. Emerald Group Publishing Limited.

Palanisamy, B., Narasimhan, B., Paul, S., Srinivasan, R., Wangpimool, W., Lim, S., Sayasane, R., 2021. Studying onset and evolution of agricultural drought in Mekong River basin through hydrologic modeling. Water 13, 3622.

Patricola, C.M., O'Brien, J.P., Risser, M.D., Rhoades, A.M., O'Brien, T.A., Ullrich, P.A., Stone, D.A., Collins, W.D., 2020. Maximizing ENSO as a source of western us hydroclimate predictability. Clim. Dyn. 54, 351–372.

Prapertchob, P., Bhandari, H., Pandey, S., 2007. Chapter 5 Economic costs of drought and rice farmers' drought-coping mechanisms in northeast Thailand. In: Pandey, S., Bhandari, H., Hardy, B. (Eds.), Economic costs of droughtand rice farmers' coping mechanisms: A cross-country comparative analysis. International Rice Research Institute, pp. 113–148.

Räsänen, T.A., Kummu, M., 2013. Spatiotemporal influences of ENSO on precipitation and flood pulse in the Mekong River basin. J. Hydrol. 476, 154–168.

Räsänen, T.A., Lindgren, V., Guillaume, J.H., Buckley, B.M., Kummu, M., 2016. On the spatial and temporal variability of ENSO precipitation and drought teleconnection in mainland Southeast Asia. Clim. Past 12, 1889–1905.

Rasmusson, E.M., Carpenter, T.H., 1982. Variations in tropical sea surface temperature and surface wind fields associated with the southern oscillation/ El Niño. Mon. Weather Rev. 110, 354–384.

Shukla, S., Wood, A.W., 2008. Use of a standardized runoff index for characterizing hydrologic drought. Geophys. Res. Lett. 35, L02405.

Singhrattna, N., Rajagopalan, B., Clark, M., Krishna Kumar, K., 2005. Seasonal forecasting of Thailand summer monsoon rainfall. Int. J. Climatol. 25, 649–664.

Son, N.T., Chen, C., Chen, C., Chang, L., Minh, V.Q., 2012. Monitoring agricultural drought in the lower mekong basin using modis ndvi and land surface temperature data. Int. J. Appl. Earth Obs. Geoinf. 18, 417–427.

Srivastava, A., Saco, P.M., Rodriguez, J.F., Kumari, N., Chun, K.P., Yetemen, O., 2021. The role of landscape morphology on soil moisture variability in semi-arid ecosystems. Hydrol. Process. 35 (1), e13990.

Tan, M.L., Gassman, P.W., Srinivasan, R., Arnold, J.G., Yang, X., 2019. A review of SWAT studies in Southeast Asia: applications, challenges and future directions. Water 11, 914.

Thilakarathne, M., Sridhar, V., 2017. Characterization of future drought conditions in the lower Mekong River basin. Weather Clim. Extrem. 17, 47–58.

Tum, K., Lai, G., Lak, D., 2016. TheDrought Crisis in the Central Highlands of Vietnam.

Vergni, L., Di Lena, B., Todisco, F., Mannocchi, F., 2017. Uncertainty in drought monitoring by the standardized precipitation index: the case study of the Abruzzo region (central Italy). Theor. Appl. Climatol. 128, 13–26.

Vu, T., Mishra, A., 2016. Spatial and temporal variability of standardized precipitation index over Indochina peninsula. Cuad. Investig. Geogr. 42, 221–232.

Vu, M., Raghavan, S.V., Liong, S.-Y., 2012. Swat use of gridded observations for simulating runoff–a Vietnam river basin study. Hydrol. Earth Syst. Sci. 16, 2801–2811.

Vu, M., Raghavan, V., Liong, S.-Y., 2015a. Ensemble climate projection for hydro-meteorological drought over a river basin in central highlandVietnam. KSCE Journal of Civil Engineering 19, 427–433.

Vu, M.T., Raghavan, S.V., Pham, D.M., Liong, S.-Y., 2015b. Investigating drought over the central highland, Vietnam, using regional climate models. J. Hydrol. 526, 265–273.

Vu, M., Vo, N., Gourbesville, P., Raghavan, S., Liong, S.-Y., 2017. Hydrometeorological drought assessment under climate change impact over the vu gia-thu Bon River basinVietnam. Hydrological Sciences Journal 62, 1654–1668.

Vu, T.M., Raghavan, S.V., Liong, S.-Y., Mishra, A.K., 2018. Uncertainties of gridded precipitation observations in characterizing spatio-temporal drought and wetness over Vietnam. Int. J. Climatol. 38, 2067–2081.

Wilhite, D.A., 2000. Chapter 1 drought as a natural hazard: concepts and definitions. Drought Mitigation Center Faculty Publications. 69.
Wilhite, D.A., Glantz, M.H., 1985. Understanding the drought phenomenon: the role of definitions. Water Int. 10, 111–120.
Wu, H., Chen, B., 2015. Evaluating uncertainty estimates in distributed hydrological modeling for the Wenjing River watershed in China by GLUE, SUFI-2, and ParaSol methods. Ecol. Eng. 76, 110–121.
Xu, Z., Takeuchi, K., Ishidaira, H., 2004. Correlation between El Niño southern oscillation (ENSO) and precipitation in south-East Asia and the pacific region. Hydrol. Process. 18, 107–123.
Xue, Z., Liu, J.P., Ge, Q., 2011. Changes in hydrology and sediment delivery of the Mekong River in the last 50 years: connection to damming, monsoon, and ENSO. Earth Surf. Process. Landf. 36, 296–308.
Yang, J., Reichert, P., Abbaspour, K.C., Xia, J., Yang, H., 2008. Comparing uncertainty analysis techniques for a swat application to the chaohe basin in China. J. Hydrol. 358, 1–23.
Yatagai, A., Kamiguchi, K., Arakawa, O., Hamada, A., Yasutomi, N., Kitoh, A., 2012. Aphrodite:Constructing a Long-term Daily Gridded Precipitation Dataset for Asia Based ona Dense Network of Rain Gauges.
Zhang, Y., Li, Z., 2020. Uncertainty analysis of standardized precipitation index due to the effects of probability distributions and parameter errors. Front. Earth Sci. 8, 76.
Zhang, B., Zhang, L., Guo, H., Leinenkugel, P., Zhou, Y., Li, L., Shen, Q., 2014. Drought impact on vegetation productivity in the lower mekong basin. Int. J. Remote Sens. 35, 2835–2856.
Zhang, X., Qu, Y., Ma, M., Liu, H., Su, Z., Lv, J., Peng, J., Leng, G., He, X., Di, C., 2020. Satellite-based operational real-time drought monitoring in the transboundary lancang-Mekong River basin. Remote Sens. 12, 376.